Molecular Biology of the Cell
Vol. 11, 2803–2820, August 2000

The Internal Phosphodiesterase RegA Is Essential for the Suppression of Lateral Pseudopods during *Dictyostelium* Chemotaxis

Deborah J. Wessels,[*] Hui Zhang,[*] Joshua Reynolds,[*] Karla Daniels,[*] Paul Heid,[*] Sijie Lu,[†] Adam Kuspa,[†‡] Gad Shaulsky,[‡] William F. Loomis,[§] and David R. Soll[*‖]

[*]Department of Biological Sciences, University of Iowa, Iowa City, Iowa 52242 [†]Department of Biochemistry and Molecular Biology, Baylor College of Medicine, Houston, TX 77030
[‡] Department of Molecular and Human Genetics, Baylor College of Medicine, Houston, TX 77030
[§]Department of Biology, University of California, San Diego, La Jolla, CA 92037

Submitted March 9, 2000; Revised May 23, 2000, and June 9, 2000; Accepted June 12, 2000
Monitoring Editor: Henry R. Bourne

Dictyostelium strains in which the gene encoding the cytoplasmic cAMP phosphodiesterase RegA is inactivated form small aggregates. This defect was corrected by introducing copies of the wild-type *regA* gene, indicating that the defect was solely the consequence of the loss of the phosphodiesterase. Using a computer-assisted motion analysis system, *regA*$^-$ mutant cells were found to show little sense of direction during aggregation. When labeled wild-type cells were followed in a field of aggregating *regA*$^-$ cells, they also failed to move in an orderly direction, indicating that signaling was impaired in mutant cell cultures. However, when labeled *regA*$^-$ cells were followed in a field of aggregating wild-type cells, they again failed to move in an orderly manner, primarily in the deduced fronts of waves, indicating that the chemotactic response was also impaired. Since wild-type cells must assess both the increasing spatial gradient and the increasing temporal gradient of cAMP in the front of a natural wave, the behavior of *regA*$^-$ cells was motion analyzed first in simulated temporal waves in the absence of spatial gradients and then was analyzed in spatial gradients in the absence of temporal waves. Our results demonstrate that RegA is involved neither in assessing the direction of a spatial gradient of cAMP nor in distinguishing between increasing and decreasing temporal gradients of cAMP. However, RegA is essential for specifically suppressing lateral pseudopod formation during the response to an increasing temporal gradient of cAMP, a necessary component of natural chemotaxis. We discuss the possibility that RegA functions in a network that regulates myosin phosphorylation by controlling internal cAMP levels, and, in support of that hypothesis, we demonstrate that myosin II does not localize in a normal manner to the cortex of *regA*$^-$ cells in an increasing temporal gradient of cAMP.

INTRODUCTION

Chemotactically directed motility is a characteristic of many cell types including phagocytic neutrophils and nerve growth cones (Tamagnone *et al.*, 1999; Hong *et al.*, 2000; Servant *et al.*, 2000). It also plays an essential role in the development of *Dictyostelium* where it can be analyzed genetically (Parent and Devreotes, 1996; Jin *et al.*, 2000). When *Dictyostelium* amoebae are washed free of nutrients and are dispersed on a substratum saturated with buffered salts solution, they undergo a complex and carefully orchestrated process of aggregation driven by chemotaxis to cAMP (Konijn *et al.*, 1967; Tomchik and Devreotes, 1981). Within a few hours after the initiation of development, a few cells begin to spontaneously emit pulses of cAMP. Cells in the immediate environment respond to each pulse of cAMP in two ways. First, they surge toward the source of the primary signal, and, second, they relay the signal by releasing more cAMP (Shaffer, 1962; Alcantara and Monk, 1974; Tomchik and Devreotes, 1981; Devreotes *et al.*, 1983). Within a few minutes extracellular phosphodiesterase activity removes the signal by extracellular hydrolysis of the cAMP (Franke

‖ Corresponding author.

and Kessin, 1992). These characteristics result in spreading, nondissipating waves of cAMP that direct cells over large distances into aggregation centers.

The shape of each outwardly radiating cAMP wave is roughly symmetric (Tomchik and Devreotes, 1981; Devreotes *et al.*, 1983), and the average period between waves during the natural aggregation process is approximately 7 min (Alcantara and Monk, 1974; Devreotes, 1982). As a cell encounters the front of a wave, it experiences an increasing spatial gradient of cAMP and an increasing temporal gradient of cAMP, while in the back of each wave a cell experiences a decreasing spatial gradient of cAMP and a decreasing temporal gradient of cAMP (Figure 1A) (Soll, 1989; Soll *et al.*, 1993). If cells simply use the spatial information of a wave in chemotaxis, we are faced with a paradox (Soll, 1989; Soll *et al.*, 1993). Since *Dictyostelium* amoebae are capable of changing direction within a few seconds in response to cAMP released from a micropipette (Gerisch *et al.*, 1975), and since both the front and the back of each wave takes > 60 s to cross them, why do they not move toward the aggregation center as they encounter the front of each wave and then move away from the aggregation center as they encounter the back of the wave? This would lead to no net movement toward the aggregation center over time. The answer lies in the manner in which the temporal dynamics of each wave regulate cell behavior and has been revealed by analyzing cell behavior in temporal gradients of cAMP (Van Haastert, 1983; Fisher *et al.*, 1989) and by simulating the temporal dynamics of a natural wave in the absence of a spatial gradient (Varnum *et al.*, 1985; Varnum-Finney *et al.*, 1987a; Wessels *et al.*, 1992; Wessels and Soll, unpublished observations).

After the first in a series of simulated temporal waves, *Dictyostelium* amoebae exhibit the following behavior in each successive wave (Figure 1B). When cAMP first starts to rise in the increasing phase of a wave, cells extend numerous pseudopods for a short period of time, then one pseudopod assumes anterior dominance (i.e., assumes the role of lead-

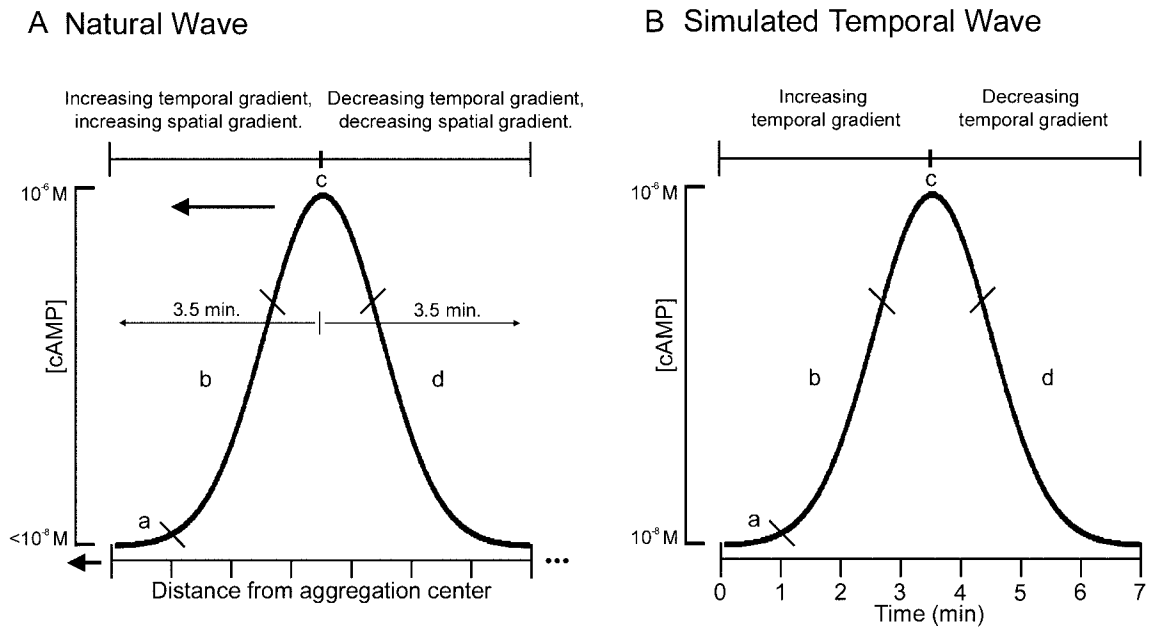

a. *Beginning of Front of Wave:* frenetic pseudopod formation in all directions.

b. *Middle of Front of Wave:* increase in velocity; suppression of lateral pseudopod formation, suppression of sharp turns; polar morphology; persistent translocation ***(in the direction of the aggregation center in the case of natural wave; in random directions in the case of simulated temporal waves).***

c. *Peak of Wave:* freeze; decrease in velocity.

d. *Back of Wave:* decreased velocity; frequent lateral pseudopod formation; apolar morphology; frequent turning in random directions; no net progress in any direction.

Figure 1. The behavior of a cell in the different portions of a natural cAMP wave propagated in a population of developing *Dictyostelium discoideum* amoebae (A) and in a temporal wave of cAMP generated in a perfusion chamber in the absence of a spatial gradient of cAMP (B). The cyclic behavior of cells responding to natural waves of cAMP is similar to that of cells responding to the different portions of a simulated wave (a, b, c, and d) in all aspects but one. While cells in the front of a natural wave all move in a persistent manner in the same direction (i.e., toward the aggregation center, the source of the wave), cells in the front of a simulated temporal wave move in a persistent manner in all directions. From the similar cyclic pattern of behaviors, the portions of the natural wave were deduced from the known portions of the in vitro generated temporal wave (Wessels *et al.*, 1992). The heavy arrow in (A) indicates the direction of spreading of the nondissipating, relayed natural wave. The bold print in point b refers to the one difference between the behavior in a natural wave and the behavior in a simulated temporal.

ing edge). Then, as the concentration continues to rise, cells become highly polar and crawl in a persistent manner because of the suppression of lateral pseudopod formation (Figure 1). At the peak of a simulated temporal wave, cells stop directional locomotion, and, in the back of the wave when the concentration of cAMP decreases with time, the cells extend lateral pseudopods in random directions, become relatively unpolarized, and move in a nonpersistent, nondirectional manner, making little net progress in any direction (Figure 1B). This complex behavior cycle is repeated in each successive simulated temporal wave. The behavior of cells in natural waves appears to be similar in most respects to that in simulated temporal waves (Figure 1) (Wessels *et al.*, 1992). As the deduced front of a natural wave crosses them and the concentration of cAMP rises, cells move in a persistent manner as they do in the front of a simulated temporal wave. Again, persistent translocation is facilitated by the suppression of lateral pseudopod formation. At the deduced peak of a natural wave, cells stop directional locomotion, and, in the deduced back of a natural wave, cells make little net progress in any direction. The only difference in behavior is directionality. In the front of a natural wave, all cells move toward the aggregation center, the source of cAMP waves (Figure 1A), while in a simulated temporal wave, cells move in all directions since they do not receive spatial cues (Figure 1B).

The gene *regA* encodes a cytoplasmic phosphodiesterase that is activated by phosphorelay from a histidine on RdeA to an aspartate in the N-terminal portion of RegA (Shaulsky *et al.*, 1996; Chang *et al.*, 1998; Shaulsky *et al.*, 1998; Thomason *et al.*, 1998). The *regA* gene is expressed shortly after the initiation of development, and its product regulates the internal concentration of cAMP throughout development (Shaulsky *et al.*, 1998). There is evidence that the MAP kinase ERK2 also controls the activity of RegA by threonine phosphorylation in the C-terminal portion of RegA (S. Lu, C. Su, B. Wang, A. Shaulsky, E. Snaar-Jagalska, and A. Kuspa; submitted). ERK2 is activated when extracellular cAMP binds to the surface receptor CAR1 (Maeda *et al.*, 1996). ERK2 appears to inhibit RegA activity leading to accumulation of internal cAMP (S. Lu *et al.*, submitted). The cAMP protein kinase PKA then would be expected to be activated. It has been proposed that PKA activity leads indirectly to the inhibition of both CAR1 and ERK2 activity, such that RegA can be reactivated and reduce the internal concentration of cAMP (Laub and Loomis, 1998). This network would lead to periodic oscillations in PKA activity as external cAMP waves transiently stimulate CAR1. The model predicts that RegA plays an essential role in generating regular periodic cAMP pulses and the entrainment of cells such that they signal in unison. Previous studies have indicated that ERK2 also is involved in both signaling and responses to cAMP (Segall *et al.*, 1995; Wang *et al.*, 1998). We have now found that RegA plays a role in the motile response of cells to natural waves of cAMP.

Using computer-assisted motion analysis systems (Soll, 1995; Soll and Voss, 1998; Wessels, 1998; Soll, 1999), the behavior of *regA*$^-$ cells has been quantitatively analyzed when cells are perfused with buffer in a chamber that excludes chemotactic signaling (Wessels *et al.*, 1989), in natural waves of cAMP (Wessels *et al.*, 1992), in a gradient chamber in which spatial gradients of cAMP are generated in the absence of the temporal dynamics of waves (Zigmond, 1977; Varnum and Soll, 1984; Varnum-Finney *et al.*, 1987b), and in temporal gradients of cAMP generated in a perfusion chamber in which spatial gradients of cAMP are not established (Varnum *et al.*, 1985; Varnum-Finney *et al.*, 1987b; Wessels *et al.*, 1992). Our results demonstrate that RegA is not involved in reading the direction of a spatial gradient or in assessing the direction (increasing versus decreasing) of a temporal wave, and responding with chemokinetic stimulation in the increasing phase. However, RegA is necessary for the suppression of lateral pseudopod formation in response to an increasing temporal gradient of cAMP, and its role appears to be in the regulation of myosin II localization in the cortex. In the absence of pseudopod suppression in the front of a wave, chemotaxis in an aggregation territory is disrupted.

MATERIALS AND METHODS

Origin of Control, regA$^-$, and regA$^-$-Rescued Strains

The isolation and original characterization of the *regA*$^-$ strain from the parent strain AX4 by saturation restriction enzyme-mediated integration (REMI) were described in a previous report (Shaulsky *et al.*, 1996). The *regA*$^-$-rescued strain was isolated by the following procedure. Genomic DNA from the 5′-end of *regA* was prepared as a 1094-bp *Hin*dIII-*Sal*I fragment, and genomic DNA from the 3′ end was prepared as a 1014-bp *Hin*dIII-*Nco*I fragment, both from the original REMI clone-out vector pSTB6-Hind (Shaulsky *et al.*, 1996). An *Sal*I–*Nco*I cDNA fragment was prepared from a full-length REGA cDNA clone (Shaulsky *et al.*, 1998). A plasmid backbone containing the neoresistance cassette was prepared as a 4730-bp *Hin*dIII fragment from pDdGa115(H^+) (Harwood and Drury, 1990). The fragments were cloned sequentially into the backbone vector using standard recombinant DNA techniques. All of the fragment junctions were verified by sequencing and by Southern analysis. The complete sequence of *regA* has been deposited in GenBank (U60170). The resulting plasmid pregAxNeo was transformed into *regA*$^-$ cells by $CaPO_4$ precipitation and glycerol shock (Nellen and Firtel, 1985), and transformants were selected using 10 μg/ml G418 in HL5 medium (Cocucci and Sussman, 1970). BlasticidinS (4 μg/ml) also was added in the medium to maintain the insertion mutation in the native *regA* locus. G418 and blasticidin-resistant transformants were cloned on SM agar in association with *Klebsiella aerogenes.* Individual colonies were randomly selected and regrown in HL5 medium plus G418 and blasticidin. Total cellular protein from each strain was prepared, and Western blot analysis was performed with polyclonal anti-RegA antibodies (Thomason *et al.*, 1998) to test for the presence of the RegA protein. One such strain, pregAxNeo/*regA*, was chosen and used for the studies reported here. Estimates from semiquantitative Western analyses indicated that this strain produced 1.5-fold wild-type levels of RegA (our unpublished results). In addition, the *regA*$^-$-rescued strain was tested for the restoration of large aggregate size (aggregates of *regA*$^-$ are abnormally small), streaming (*regA*$^-$ cells do not stream), and normal levels of cAMP after cAMP stimulation (*regA*$^-$ cells have threefold to fourfold more cAMP than Ax4 cells) (Lu *et al.*, 2000).

Maintenance and Development of Control, regA$^-$, and Rescued Strains

Spores of the parental Ax4 strain, the *regA*$^-$ strain, and the rescued *regA*$^-$ strain were frozen in 10% glycerol at −80°C and were reconstituted every 3 wk for experimental purposes (Sussman, 1987). Cells were grown in suspension in HL-5 medium to a density of 2×10^6 cells/ml. To initiate development, cells were washed free of

nutrients in basic salts solution (BSS; 20 mM KCl, 2.5 mM $MgCl_2$, and 20 mM KH_2PO_4 [pH 6.4]) and then were dispersed onto filter pads as a smooth carpet at a density of 5×10^6 cells/cm^2 (Soll, 1987). For motility experiments in buffer, and in spatial and temporal gradients of cAMP (see below), cells were harvested at the ripple stage, which represents the onset of aggregation (Soll, 1979).

Analysis of Cell Motility in a Spatial Gradient of cAMP

Cells were washed from filters at the ripple stage of development and were deposited on the bridge of a Plexiglas gradient chamber as a dilute suspension in BSS according to methods previoiusly described (Varnum and Soll, 1984; Varnum-Finney *et al.*, 1987b). One trough of the chamber was immediately filled with BSS alone and the other with BSS containing 10^{-6} M cAMP, and the chamber was covered with a coverslip. The chamber was incubated undisturbed on the stage of a Leitz (Leica Microsystems, Deerfield, IL) microscope equipped with brightfield optics and a 25× objective for 5–7 min to allow the gradient to become established and for cells to reestablish adherence and motile behavior. Fields of cells were videorecorded through a DAGE camera (DAGE-MTI, Michigan City, IN) onto half-inch videotape for 10 min. The images were processed using the camera control panel so that the cells appeared dark against a lighter background, thus allowing automatic edge detection by the threshold method in 2D DIAS (Soll, 1995; Soll and Voss, 1998). Video images were digitized at a rate of 15 frames/min onto the hard disk of a PowerComputing PowerTower Pro 225 computer (Apple Computer, Cupertino, CA) equipped with a Data Translation framegrabber board (Data Translation Inc., Marlboro, MA) and 2D-DIAS software (Soll, 1995; Soll and Voss, 1998). Only those cells crawling at average velocities >3 μm/min for the 10-min period of analysis were used to compute motility parameters. This represented >80% of cells on the chamber bridge for all three cell types.

Analysis of Cell Motility in Buffer or in Simulated Temporal Waves of cAMP

To monitor the behavior of individual amoebae in buffer, 1 ml of a dilute suspension of cells at the ripple stage of development was inoculated into a Sykes-Moore chamber (Bellco Glass, Vineland, NJ) as previously described (Varnum *et al.*, 1985; Varnum-Finney *et al.*, 1987a). This perfusion chamber consisted of a rubber o-ring sandwiched between two glass coverslips within a stainless steel holder. Immediately after inoculation, the chamber was closed. Cells were allowed to settle and to adhere to the coverslip, a process that took ~5 min. The chamber then was inverted and placed on the stage of a Leitz upright microscope fitted with a long-range condenser. The chamber had one inlet and one outlet port at opposite sides of the metal ring wall. The tube to the inlet port was connected to a reservoir containing the proper perfusion solution, and the tube to the outlet port was connected to a peristaltic pump set to a flow rate of 4 ml/min, so that chamber volume was replaced every 15 s. For behavior in the absence of cAMP, cells were continuously perfused with BSS. To simulate temporal waves of cAMP, amoebae were perfused with increasing, then decreasing, temporal step-gradients of cAMP. In each experiment, amoebae first were perfused with 5 ml of BSS solution lacking cAMP and then with 2 ml of fresh BSS solution containing 7.8×10^{-9} M cAMP. Then at 30-s intervals, 2 ml of a new solution was perfused that contained twice the cAMP concentration of the preceding solution. After perfusion with 2 ml of the buffer solution containing 10^{-6} M cAMP (the peak concentration), the last step in the increasing gradient, the decreasing temporal gradient was simulated by introducing 2-ml increments of BSS into the reservoir, each containing one-half the previous concentration of cAMP. The second, third, and fourth waves were created using this same technique. The rapid flow rate and round shape of the chamber prevented the establishment of spatial gradients of cAMP, and this was verified using fluorescent dyes. Fields of cells were videorecorded, and the cell images were processed and digitized as described above.

Analysis of Cell Motility in Natural Waves of cAMP

For analyzing behavior in natural aggregation territories, exponentially growing cells were washed free of nutrients and were suspended in BSS at 2.4×10^6 cells/ml according to methods previously described (Escalante *et al.*, 1997) with one exception. Two milliliters of the cell suspension were added to the uncoated surface of a 35-mm tissue culture dish. Dishes were used without an agar coating because the particular strain employed (Ax4) adhered more securely to the plastic surface than previous strains used for similar studies (Wessels *et al.*, 1992; Escalante *et al.*, 1997). After a 30-min incubation period, the cells had settled and had attached to the surface. One milliliter of fluid was carefully withdrawn, and the dish was placed on the stage of a Zeiss ICM 405 inverted microscope (Carl Zeiss, Thornwood, NY). Images were recorded through a Hamamatsu C-2400 Newvicon camera (Hamamatsu Photonics, Hamamatsu City, Japan) using a 10 X objective and brightfield optics. Video images were digitized at a rate of 6 frames/min as described above.

Labeling Cells with DiI and Mixing with Unlabeled Cells

To test the behavior of mutant cells in wild-type aggregation territories, *regA*$^-$ cells were stained with the vital dye DiI (Molecular Probes, Eugene OR), mixed with a majority of unlabeled Ax4 cells, and motion analyzed during aggregation. To label *regA*$^-$ amoebae, 8×10^6 cells in the log-phase of growth were pelleted, washed three times in BSS, and then resuspended in 2 ml of labeling solution (3% dextrose in BSS). A 4 mM stock solution of DiI in ethanol was stored at −20°C. Before use, the stock solution of DiI was passed through a 5-μm filter, and then 25 μl of the filtrate was added to the cell suspension to give a final concentration of 0.05 mM DiI. *regA*$^-$ cells were incubated in the DiI solution for 30 min, washed three times in BSS, and then mixed with unlabeled Ax4 cells at a ratio of 1:4. Ax4 cells were prestarved for 2 h before mixing so that the developmental timing of the two strains would be comparable (see Results section). Labeled and unlabeled cells were mixed, and 5×10^6 cells were dispersed evenly on the surface of a 35-mm Petri dish. The Petri dish was placed on the stage of an Axiovert 100STV Zeiss microscope (Carl Zeiss) and examined with a NORAN laser scanning confocal microscope (NORAN, Middleton, WI). The same procedure was used to test the behavior of wild-type cells in mutant aggregation territories. Transmitted light images were continuously collected through a transmitted light detector. Settings in Oz Intervision Software (NORAN) were selected so that cells were exposed to laser light for 0.5 s every 20 s with a laser intensity of 20%, at an excitation of 568 nm and an emission ≥590 nm. Transmitted and fluorescent images were collected through the photomultiplier tube, were mixed and averaged using the Intervision Software, and then were saved on the hard drive in Silicon Graphics (SGI, Inc., Mountain View, CA) movie format. The transmitted and fluorescent imaging format functioned automatically throughout aggregation. SGI movies acquired with the NORAN system were converted to Quick Time format, and labeled cells were outlined using 2D-DIAS (see below).

Two Dimensional Computer-Assisted Analysis of Cell Motility

Digitized images of cells in buffer, in spatial gradients of cAMP, in simulated temporal waves of cAMP, or in natural waves of cAMP were image processed, and the perimeters of cells were automatically outlined using the grayscale threshold option of DIAS (Soll,

1995; Soll and Voss, 1998). Perimeters were converted to beta-spline replacement images, which were used to compute the position of the centroid (Soll, 1995; Soll and Voss, 1998). Motility parameters were computed from centroid positions, and dynamic morphology parameters were computed from the perimeter contours of the replacement images according to formulas derived and discussed in a previous report (Soll, 1995). In brief, "instantaneous velocity" of a cell in frame n was computed by drawing a line from the centroid in frame n − 1 to the centroid in frame n + 1 and then dividing the length of the line by twice the time interval between analyzed frames. "Directional change" was computed as the direction in the interval (n − 1, n) minus the direction in the interval (n, n + 1). If directional change was >180°, it was subtracted from 360°, resulting in a positive value between 0° and 180°. "Positive flow" was computed from difference pictures (Soll, 1995; Soll and Voss, 1998). To generate a difference picture, the cell perimeter in frame n was superimposed on the perimeter in frame n − 1. The regions in the image in frame n not overlapping the image in frame n − 1 were considered "expansion zones" and were color-coded green. The regions in the image in frame n − 1 not overlapping the image in n were considered "contraction zones" and were color-coded red. The summed area of expansion zones divided by the total cell area in frame n times 100 represents positive flow in microns squared per interval time. "Maximum length" was computed as the longest chord between any two points along the perimeter, and "maximum width" as the longest chord perpendicular to maximum length. "Roundness" was computed by the formula $100 \times 4\pi$ (area/perimeter squared). "Convexity" and "concavity" were computed by first drawing line segments connecting the vertices of the final cell shape. The angles of turning from one segment to the next were measured. Counterclockwise turns were positive, and clockwise turns were negative. Convexity was computed as the absolute value of the sum of positive turn angles, in degrees, and concavity was computed as the absolute value of the sum of negative turn angles. The "chemotactic index" was computed as the net distance moved to the source of chemoattractant divided by the total distance moved in the time period. "Percent positive chemotaxis" was computed as the proportion of the cell population exhibiting a positive chemotactic index.

Quantitative Immunolocalization of Myosin II in the Front of a Temporal Wave

To quantitate the distribution of myosin II in cells responding to the front of a simulated temporal wave of cAMP, Ax4 or *regA*$^-$ cells were washed from filters at the ripple stage of development, were inoculated into a Sykes–Moore chamber, and were treated with successive simulated temporal waves of cAMP, as detailed above. Midway through the third wave, the chamber was perfused with freshly prepared 4% paraformaldehyde in PBS supplemented with 0.01% saponin. The cells were fixed for 10 min at room temperature. The chamber was disassembled, and the coverslip was gently washed with TBS. Before immunostaining, antigen retrieval was performed using Target Retrieval Solution (DAKO Corp., Carpinteria, CA) in a steamer and processed for 20 min in retrieval solution heated to 90°C. The solution and coverslips were removed from heat and were allowed to cool to room temperature before TBS rinsing. Nonspecific binding was blocked with 10% normal donkey serum in PBS. To localize myosin II, cells were incubated with rabbit antimyosin II antibody (1/1000), a generous gift from Dr. Arturo De Lozanne (University of Texas at Austin, Austin, TX) in PBS containing 10% donkey serum for 45 min at 37°C. After extensive PBS rinsing, cells were stained with FITC-labeled donkey anti-rabbit antibody (1/200) (Jackson ImmunoResearch, West Grove, PA) for 30 min at room temperature. Coverslips were rinsed and mounted using Gelvatol (Monsanto Corp., St Louis, MO) with azide. Images were captured with a Zeiss 510 laser-scanning confocal microscope (LSM 510; Central Microscopy Facility, University of Iowa). For quantitative analysis, an initial image was scanned using an Ax4 cell, and the parameters were optimized. These same parameters then were used for each subsequent scan. The same scanning parameters were used for *regA*$^-$ cells. LSM 510 software was used to convert 2D optical slices into filled "Pseudo 3D" projections in which the *z*-axis represents the grayscale intensity distribution over the scanned area.

RESULTS

Rescue of regA$^-$ Phenotypes by the Wild-Type Gene

Strains in which *regA* is disrupted form only small aggregates and develop into misshapen fruiting bodies (Shaulsky *et al.*, 1996, 1998). To be sure that this aberrant behavior was directly related to the loss of RegA, we transformed mutant cells with a vector carrying the *regA* coding region and its upstream regulatory sequence (see MATERIALS AND METHODS). Stable transformants formed large aggregation streams and developed into normal fruiting bodies, while the parent *regA*$^-$ strain failed to stream and formed small aberrant fruiting bodies in the midst of aggregates that did not complete morphogenesis (Figure 2). These results demonstrate that the aberrant behavioral phenotype of *regA*$^-$ cells can be attributed to the specific loss of *regA*. The defect in aggregation could result from reduced motility, defective chemotactic signaling, or a defective behavioral response to cAMP waves.

Basic Motility of regA$^-$ Cells

The velocity of individual cells changes during the early developmental stages of *Dictyostelium* (Varnum *et al.*, 1985; Shutt *et al.*, 1995). The instantaneous velocity of cells is low at the beginning of the developmental program, increases to a peak value at the onset of aggregation, and then decreases through the later stages of development. During the preaggregative period, the instantaneous velocity of individual Ax4 cells continually increased from 2 to 10 μm/min at the onset of aggregation, then decreased during the later stages of aggregation (Figure 3A). Motility was developmentally regulated in a similar manner in *regA*$^-$ cells (Figure 3B). Aggregation began 2 h earlier in *regA*$^-$ cultures than in Ax4 cultures, and peak instantaneous velocity also was achieved 2 h earlier (compare Figure 3, A and B). Therefore, in the comparative studies that follow, cells of the three test strains (Ax4, *regA*$^-$, and *regA*$^-$-rescued) were obtained from developing cultures at the observed onset of aggregation (i.e., the ripple stage; Soll, 1979).

The quantitative parameters of motility of individual Ax4 and *regA*$^-$ cells translocating in buffer without added cAMP were similar. Ax4 and regA$^-$ cells translocated with mean instantaneous velocities (±SD) of 10.8 ± 3.9 and 11.1 ± 4.2 μm/min, respectively, and with mean directional change parameters (±SD) of 44.3° ± 7.9° and 51.0° ± 6.3° per minute, respectively (Table 1). Mean cell shape parameters, including mean maximum length and mean roundness, were also similar (Table 1). These results indicate that RegA plays no role in the basic motile behavior of *Dictyostelium* amoebae translocating in the absence of a chemoattractant.

Both the Generation and Response to Natural Waves of cAMP Are Impaired in regA$^-$ Cells

To assess the behavior of cells in natural aggregation territories, Ax4 or *regA*$^-$ cells were dispersed on the surface of tissue culture dishes, and the behavior of neighboring cells

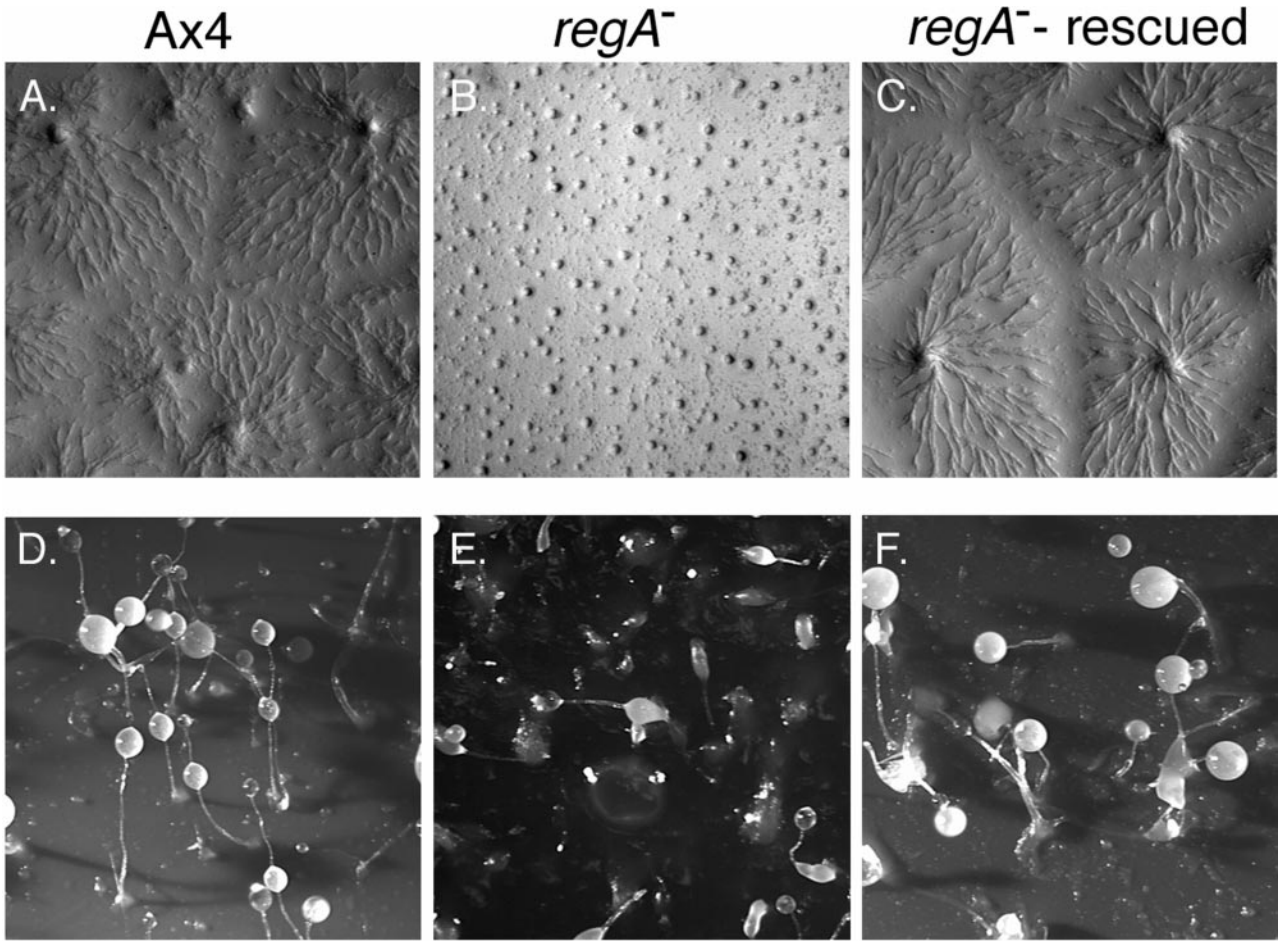

Figure 2. The late aggregation territories (A–C) and fruiting bodies (D–F) of Ax4, *regA*$^-$, and *regA*$^-$-rescued cell cultures, respectively. Note the abnormally small size (B) as well as the absence of streams (B) and the incomplete or small fruiting bodies (E) in *regA*$^-$ cultures. Note the reexpression of normal traits, including large aggregates and streaming (C) and large fruiting bodies (F) in *regA*$^-$-rescued cultures.

was continually videorecorded through the aggregation process in submerged cultures (Wessels *et al.*, 1992; Escalante *et al.*, 1997). In Figure 4,A–C, the time plots of instantaneous velocity and corresponding centroid tracks are presented for three representative Ax4 amoebae that were near each other in the same localized area of an aggregation territory. For these three independent, neighboring cells, the instantaneous velocity plots contained sharp peaks with average periods (±SD) between peaks of 5.8 ± 1.3, 5.9 ± 1.5, and 5.9 ± 1.9 min, respectively. The velocity peaks have been interpreted to represent periods of rapid, persistent movement in the front of consecutive natural waves, while velocity troughs have been interpreted to represent the behavior at the peak and in the back of the consecutive waves (Figure 1A) (Wessels *et al.*, 1992). Average peak instantaneous velocities (±SD) for the three representative cells were 5.3 ± 0.9, 5.7 ± 1.0, and 5.5 ± 1.1 μm/min, respectively, and the ratios of average peak to trough velocity values were 2.4, 2.3, and 2.2, respectively (Figure 4, A–C). Portions of the centroid track of each cell representing peak and trough velocities were easily distinguished by the expanded and contracted distances, respectively, between centroids (Figure 4, A–C). More importantly, through sequential waves each Ax4 cell moved in a directed manner toward the same aggregation center. Similar behavior was observed for nine additional sets of spatially associated Ax4 amoebae in the process of aggregation.

In Figure 4, D–F, time plots of instantaneous velocity and corresponding centroid tracks are presented for three aggregating *regA*$^-$ amoebae that were near each other in the same localized area of a culture dish. As in the case of Ax4 cells, the time plots of instantaneous velocity were cyclic, but the period and peak velocities were less regular. For these three *regA*$^-$ cells, the average periods (±SD) were 3.9 ± 0.8, 5.2 ± 1.9, and 3.9 ± 0.2 min, respectively. In repeat experiments, more variability was evident in the average period between velocity peaks of *regA*$^-$ cells than in those of wild-type Ax4 cells. In fact, within each of the 10 sets of spatially localized Ax4 amoebae undergoing aggregation that were motion analyzed, there was no significant difference in periodicity. This result suggests that *regA*$^-$ cells may not be responding to the same source of chemotactic signals even when they are in close spatial proximity.

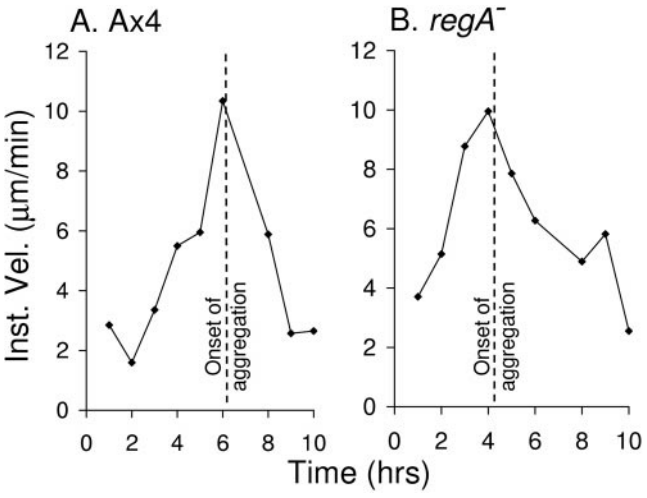

Figure 3. Motility is developmentally regulated in *regA*$^-$ cells (B) as it is in parental Ax4 cells (A). Cells were removed from the respective developing cultures at the noted intervals, were dispersed on the wall of a perfusion chamber, and average instantaneous velocity were measured over a 10-min period. The mean instantaneous velocity at each time point was computed from the average instantaneous velocities of 20 amoebae at each time point.

The average trough values of instantaneous velocity for the three *regA*$^-$ cells (Figure 4, D–F) were similar to those for the three Ax4 cells (Figure 4, A–C). However, the average peak values were consistently lower for the three *regA*$^-$ cells than those for the three Ax4 cells. While the peak to trough ratio of the three representative *regA*$^-$ cells was 1.4 in each case, the ratios of the three Ax4 cells were 2.4, 2.3, and 2.2, respectively. These results suggest that in a developing culture, *regA*$^-$ cells appear to release cAMP and respond to it, but they fail to achieve the high peak velocities of Ax4 cells.

In contrast to the relatively straight paths taken by Ax4 cells (Figure 4, A–C), *regA*$^-$ cells zig-zagged and backtracked (Figure 4, D–F). For the three spatially localized *regA*$^-$ cells that were motion analyzed, no single direction reflecting the position of an aggregation center could be discerned. This aberrant behavior no doubt accounts for the very small aggregates formed by *regA*$^-$ cells (Shaulsky *et al.*, 1998). In addition, while the periods of translocation representing peak and trough velocities were easily distinguished in centroid tracks of Ax4 cells (Figure 4, A–C), they were not as easily distinguished in centroid tracks of *regA*$^-$ cells (Figure 4, D–F), primarily because the peak velocities of *regA*$^-$ cells were in many cases depressed and the tracks were not as persistent and directional during periods of increased velocity.

The aberrant behavior of *regA*$^-$ cells could be the result of an abnormality in the genesis of waves, an abnormality in the response to waves, or both. To distinguish between these three possibilities, experiments were performed in which DiI-labeled cells of one cell type were mixed with a majority of unlabeled cells of the other type. The fluorescent dye DiI did not affect motility, since centroid tracks and velocity plots of labeled and unlabeled AX4 cells mixed at a ratio of 1 to 4 were not significantly different (our unpublished results).

In Figure 5A, the time plot of instantaneous velocity and the centroid track are presented for a representative unlabeled *regA*$^-$ cell in an aggregation territory that contained 20% DiI-labeled Ax4 cells and 80% unlabeled *regA*$^-$ cells. The velocity plot of the *regA*$^-$ cell was generally depressed, and the centroid track was compressed and directionless (Figure 5A) in a manner that was similar to that of *regA*$^-$ cells in homogeneous *regA*$^-$ territories (Figure 4, D–F). The peak velocities in the time plots of labeled Ax4 cells in the same *regA*$^-$ territory (Figure 5, B and C) were higher than those of *regA*$^-$ cells, more similar in fact to those of Ax4 cells in Ax4 territories (Figure 4, A–C). However, the centroid tracks of these Ax4 cells, although expanded, exhibited no discernable directionality (Figure 5, B and C). These results, obtained in several repeat experiments, suggest that although cAMP appears to be released in a pulsatile manner in territories containing 80% *regA*$^-$ cells and 20% Ax4 cells, the signals are not propagated from a single aggregation center even in a restricted part of the territory. Since *regA*$^-$ cells make up the majority of cells in these territories, it appears they may not be entrained to relay the signal coordinately. In addition, the suppressed velocity peaks in instantaneous velocity plots of *regA*$^-$ cells (Figure 5A), when compared with those of Ax4 cells (Figure 5, B and C) in *regA*$^-$ territories, suggest an aberrant behavioral response by *regA*$^-$ cells to cAMP signals.

To test whether the response of *regA*$^-$ cells to a natural cAMP wave was defective, the behavior of DiI-labeled *regA*$^-$ cells was analyzed in territories of unlabeled Ax4 cells in which the two cell types were mixed at a ratio of 1:4, respectively. In Figure 5D, the time plot of instantaneous velocity and the centroid track are presented for an unlabeled Ax4 cell in the mixed aggregation territory. The time plot was similar to that of unlabeled Ax4 cells in homogeneous Ax4 territories (Figure 4, A–C) and included high

Table 1. A computer-assisted comparison of the motile behavior of *regA*$^-$ and Ax4 cells perfused with buffer in the absence of chemoattractant

Cell type	Cell no.	Instantaneous velocity (μm/min)	Directional change (degree/min)	Maximum length (μm)	Maximum width (μm)	Roundness (%)
Ax4	10	10.8 ± 3.9	44.3 ± 7.9	21.2 ± 4.1	10.4 ± 1.8	50.3 ± 13.2
regA	9	11.1 ± 4.2	51.0 ± 6.3	22.3 ± 3.5	10.9 ± 1.3	46.8 ± 15.2

The behavior of each cell was analyzed for 10 min. Images were digitized at 15-s intervals. Values are given as mean ± SD. The five measured parameters proved statistically indistinguishable between the two cell types using the Student's *t* test. All p values were above 0.05.

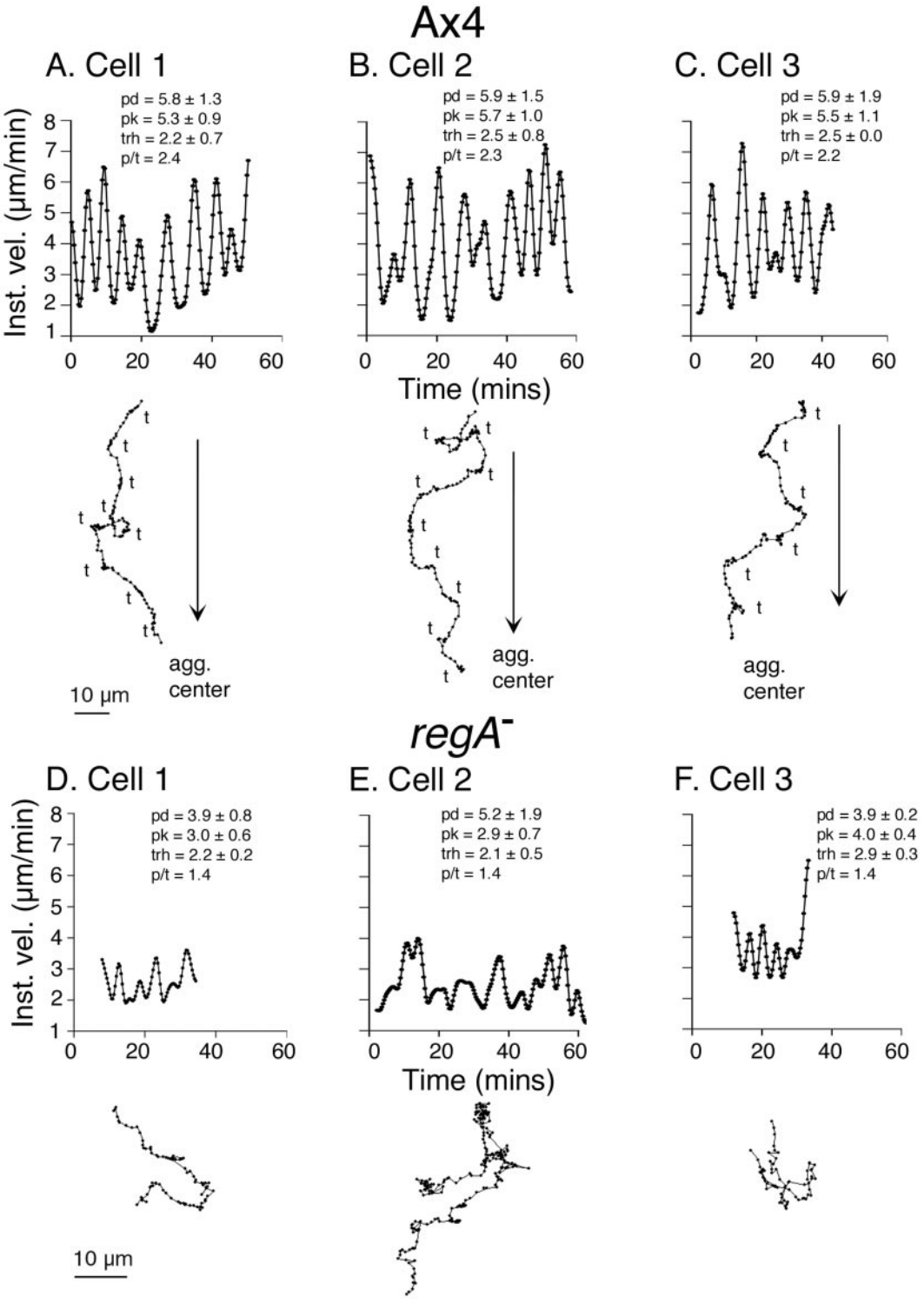

Figure 4. Time plots of instantaneous velocity and corresponding centroid tracks of three representative Ax4 cells (A–C) and three representative *regA*$^-$ cells (D–F) responding to natural waves generated in their own homogeneous aggregation territories. Arrows along Ax4 centroid tracks represent the direction toward the common aggregation center (source of waves), and "t" represents the trough regions in the respective velocity plots. In *regA*$^-$ territories, there was no single direction reflecting the source of the wave, hence no arrows have been included in panels D–F. Pd, average period between velocity peaks; pk, average peak velocity; trh, average trough velocity; p/t, ratio of average peak to average trough velocities. Values are presented as average ± SD. Velocity plots were smoothed 10 times with Tukey windows of 10, 20, 40, 20, and 10.

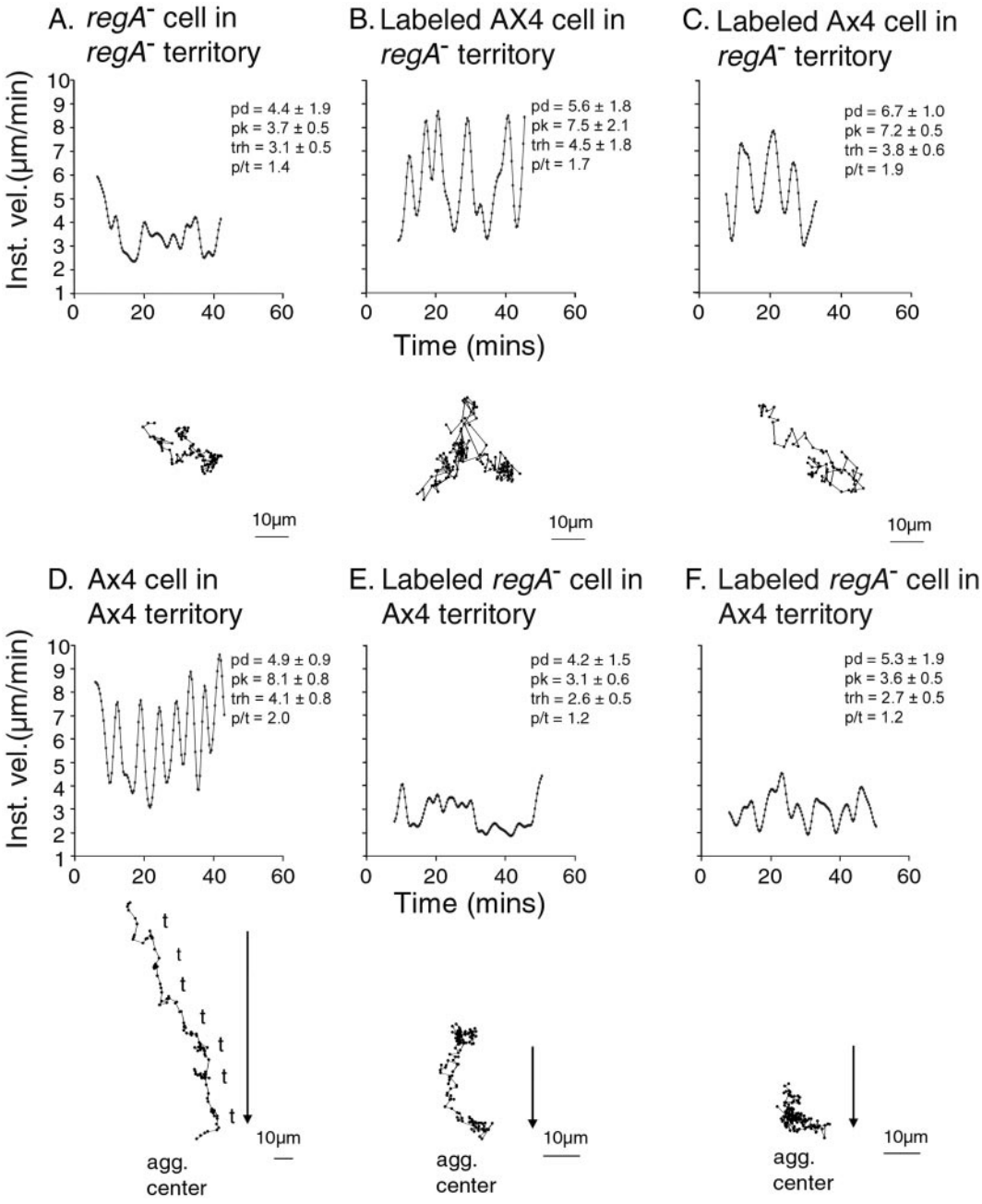

Figure 5. The behavior of a representative unlabeled *regA*$^-$ cell (A) and two DiI-labeled Ax4 cells (B and C) in the same area of a developing *regA*$^-$ culture, and the behavior of a representative unlabeled Ax4 cell (D) and two DiI-labeled *regA*$^-$ cells (E and F) in the same Ax4 aggregation territory. Arrows in (D–F) indicate the direction toward the aggregation center (the source of waves) of the territory in which the three representative cells are located. pd, pk, trh, and p/t and the smoothing regime are described in the legend to Figure 3.

average peak velocity values at regular intervals and a high peak-to-trough velocity ratio. In addition, the centroid track included discernable peak and trough velocity periods and a high degree of net directionality toward the aggregation center (Figure 5D). In contrast, the velocity plots of two labeled *regA*$^-$ cells (Figure 5, E and F) in close spatial association with the Ax4 cell followed in Figure 5D were depressed. Peak velocities and the ratios of average peak-to-trough velocities were similar to those of *regA*$^-$ cells in homogeneous *regA*$^-$ territories (Figure 4, D–F). In addition, the centroid tracks were compressed and lacked direction. Zig-zagging was rampant (Figure 5, E and F), demonstrating that the *regA*$^-$ cells did not respond with persistent translocation to the front of natural waves of cAMP. These results,

Table 2. 2D motility and dynamic morphology parameters of wild-type (Ax4), *regA*$^-$, and *regA*$^-$-rescued cells in a spatial gradient of cAMP

Cell type	Number of cells	Instantaneous velocity (μm/min)	Positive flow (%/min)	Directional change (deg/min)	Maximum length (μm)	Maximum width (μm)
Wild type (Ax4)	33	10.6 (±4.1)	8.5 (±2.5)	21.6 (±11.1)	21.5 (±3.4)	8.5 (±1.2)
regA$^-$	29	12.1 (±5.2)	8.8 (±2.9)	26.8 (±15.5)	23.7 (±5.3)	9.0 (±1.1)
regA$^-$-rescued	20	10.1 (±4.7)	7.2 (±2.0)	21.7 (±9.2)	23.4 (±5.2)	9.2 (±2.0)

Cell type	Number of cells	Area (μm^2)	Roundness (%)	Mean convexity (degree)	Mean concavity (degree)	Chemotactic index	Positive chemotaxis (%)
Wild type (Ax4)	33	119 (±17)	51.4 (±8.8)	574 (±69)	215 (±70)	+0.61 (±.34)	90
regA$^-$	29	127 (±36)	56.0 (±11.4)	583 (±84)	228 (±86)	+0.48 (±0.28)	93
regA$^-$-rescued	20	135 (±43)	51.1 (±11.0)	610 (±95)	250 (±95)	+0.67 (±0.34)	85

Parameters were computed over a 5–10-min period for each cell. In all cases, the mean (± SD) value of each parameter is for the number of cells noted. All measured parameters but the chemotactic index proved statistically indistinguishable among the three cell types, using the Student's *t* test or a one-tailed test of the null hypothesis, when the distributions were non-Gaussian. All p values for the former parameters were above 0.05. The p values for the chemotactic index between *regA*$^-$ and either wild-type (Ax4) or *regA*$^-$-rescued cells was <0.05.

obtained in several repeat experiments, demonstrate that *regA*$^-$ cells are defective not only in generating coordinated cAMP waves, but also in responding to natural cAMP waves.

Chemotaxis in Spatial Gradients of cAMP

The aberrant behavior of *regA*$^-$ cells in natural cAMP waves propagated by Ax4 cells could be because of their inability to read a spatial gradient and/or their inability to respond to the temporal dynamics of the wave (Wessels *et al.*, 1992). To distinguish between these possibilities, we first tested whether *regA*$^-$ cells could assess the direction of a spatial gradient of cAMP in the absence of the temporal dynamics of the wave and whether they could crawl in a directed manner up the gradient. Ax4 or *regA*$^-$ cells were dispersed on the Plexiglas bridge of a gradient chamber (Zigmond, 1977; Varnum and Soll, 1984; Varnum-Finney *et al.*, 1987b). To one trough, BSS solution alone was added (the "sink"), and to the other trough, BSS containing 10^{-6} M cAMP was added (the "source") (Varnum and Soll, 1984; Varnum-Finney *et al.*, 1987b). Cells were incubated for 5 min to allow the gradient to develop (Shutt *et al.*, 1998; Shutt and Soll, 1999) and to allow the cells to reestablish polarity and motility. Their behavior then was recorded and motion analyzed. There were no significant differences among Ax4, *regA*$^-$, and *regA*$^-$-rescued cells in instantaneous velocity and positive flow in a spatial gradient of cAMP, and although the directional change parameter was slightly higher in *regA*$^-$ cells, it was not significantly different (Table 2). There was also no significant difference in mean morphology parameters in a spatial gradient, including maximum length, maximum width, area, roundness, convexity, and concavity (Table 2). More importantly, the majority of *regA*$^-$ cells (93%) exhibited a positive chemotactic index, as did Ax4 (90%) and *regA*$^-$-rescued (85%) cells (Table 2). The mean chemotactic index (CI) (±SD) of *regA*$^-$ cells was +0.48 ± 0.28, which represents a relatively strong response. However, this value was lower than the mean CI (±SD) of either Ax4 cells (+0.61 ± 0.34) or *regA*$^-$-rescued cells (+0.67 ± 0.34). This difference was statistically significant (Table 2). A histogram of CIs for the three cells revealed that fewer *regA*$^-$ cells achieved top-end chemotactic indices (i.e., ≥0.80) than either Ax4 or *regA*$^-$-rescued cells (Figure 6). While 36 and 40% of Ax4 and *regA*$^-$-rescued cells exhibited CIs of ≥0.80, only 14% of *regA*$^-$ cells exhibited CIs in this high-end category.

To investigate further the behavioral basis of this difference, the perimeter tracks of chemotaxing Ax4 and *regA*$^-$ cells with the highest CIs were compared. The perimeter tracks of the highest end Ax4 cells were highly persistent in the direction of the gradient, with few lateral pseudopod projections and virtually no significant turns (Figure 7A). The perimeter tracks of the highest end *regA*$^-$ cells were also persistent in the direction of the gradient but exhibited more frequent lateral pseudopod activity and more frequent changes in direction (see arrows, Figure 7B). Together, these results demonstrate that *regA*$^-$ cells are capable of assessing the direction of a spatial gradient of cAMP and moving in a directed manner, but they are not as efficient as Ax4 cells in suppressing lateral pseudopod formation and turns, a behavioral characteristic that increases proportionately with increasing CI (Varnum-Finney *et al.*, 1987b).

Responses to Temporal Gradients of cAMP

Since the abnormal behavior exhibited by *regA*$^-$ cells in a natural wave does not appear to result from a defect in their ability to read the spatial gradient, it may instead be because of an incapacity to respond to the temporal dynamics of a natural wave, in particular the increasing phase in the front of the wave. To test this possibility, cells were subjected to sequential temporal waves of cAMP that approximated the temporal dynamics of natural waves in the absence of established spatial gradients (Varnum *et al.*, 1985; Varnum-Finney *et al.*, 1987a). In Figure 8A, the average instantaneous velocities of 10 representative Ax4 cells and 10 representative *regA*$^-$ cells are plotted while they were subjected to four

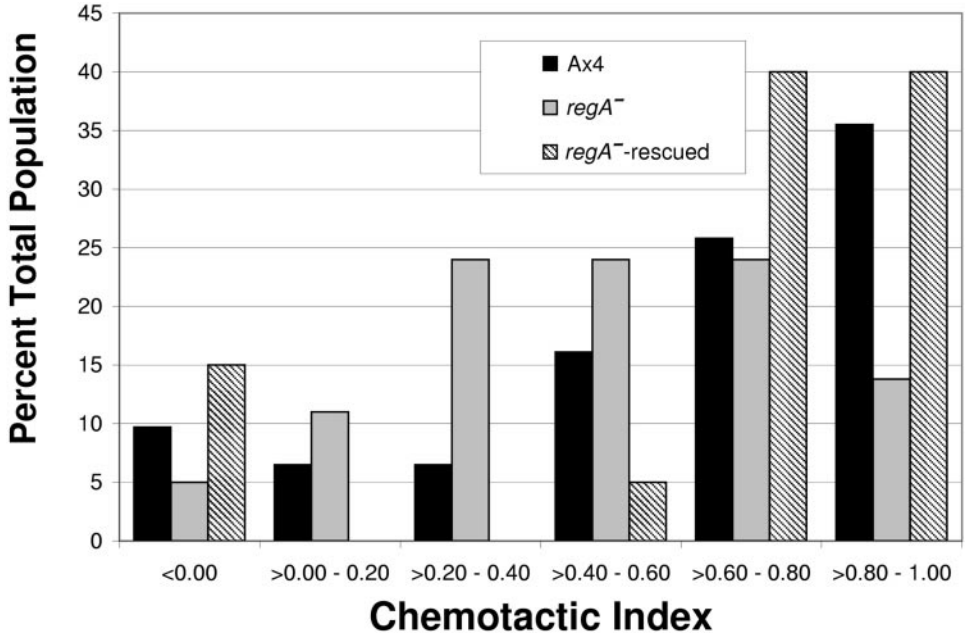

Figure 6. Histogram of CIs indicates that *regA*$^-$ cells are less efficient at attaining high-end CIs (i.e., >0.80–1.00) than either Ax4 or *regA*$^-$-rescued cells.

temporal waves of cAMP generated in sequence. As previously reported for wild-type cells (Varnum *et al.*, 1985), the instantaneous velocity of parental Ax4 and *regA*$^-$ cells remained low throughout the first wave. In subsequent waves, instantaneous velocity increased through the first half of each increasing phase, reflecting positive chemokinesis, and then decreased to a depressed level through the peak and the decreasing phase (Figure 8A). The chemokinetic responses shown by *regA*$^-$ cells were not significantly different from those of Ax4 cells, indicating that *regA*$^-$ cells recognize temporal changes in cAMP (increasing versus decreasing concentration with time) and respond by altering their instantaneous velocity accordingly, in particular by positive chemokinesis in the front of each of a series of simulated waves, beginning with the second wave. However, the centroid tracks of *regA*$^-$ cells in simulated waves were abnormal. The centroid tracks of Ax4 cells contained expanded stretches representing rapid, persistent, and directional translocation in the first two-thirds of the increasing phase of waves 2, 3, and 4, and intervening compacted stretches representing depressed rates of translocation at the peak and in the decreasing phase of each wave (Figure 8, B and C). In contrast, the centroid tracks of *regA*$^-$ cells were far more compressed, with less persistent stretches, and included constant backtracking, which indicated a higher frequency of sharp turns (Figure 8, D and E). The persistent and directional phases of translocation exhibited by Ax4 cells in the first half to two-thirds of the increasing phase of simulated waves 2, 3, and 4 were, therefore, absent in the *regA*$^-$ tracks.

Suppression of Lateral Pseudopod Formation as cAMP Increases with Time

Wild-type cells suppress lateral pseudopod formation during rapid translocation in the increasing phase of each simulated temporal wave to achieve a high degree of persistent and directional translocation (Varnum-Finney *et al.*, 1987a). Since *regA*$^-$ cells turned frequently during this phase of a temporal wave, it seemed reasonable to hypothesize that they might be impaired in this response. To test this possibility, we recorded cells responding to the increasing phases of consecutive temporal waves 2, 3, and 4 at high magnification to directly measure the frequency of lateral pseudopod formation. Lateral pseudopods were defined as protrusions representing ≥5% of the total area of the cell, which extended at an angle of ≥ 45° from the translocation axis of the cell (Wessels *et al.*, 1996). The translocation axis was determined by a line drawn between the centroids of the cell in the present frame and the frame 16 s earlier. While Ax4 cells rarely formed lateral pseudopods in the increasing phases of temporal cAMP waves (0.7 ± 0.7 per front of wave), *regA*$^-$ cells formed lateral pseudopods at a frequency five times higher (3.6 ± 1.2 per front of wave) (Table 3). The difference in the frequency of lateral pseudopod formation is evident in perimeter plots and difference pictures of representative Ax4 and *regA*$^-$ cells responding to the first two-thirds of a simulated temporal wave of cAMP (Figure 9). While Ax4 cells maintained a highly polar morphology with rare lateral extensions (Figure 9, A and C), *regA*$^-$ cells continually extended lateral pseudopods at high frequency (Figure 9, B and D). These results demonstrate that although *regA*$^-$ cells recognize temporal changes in cAMP (increasing versus decreasing concentration with time) and respond by altering their instantaneous velocity, they do not suppress lateral pseudopod formation during the increasing phases of simulated temporal waves, resulting in a loss of persistent, directional translocation.

regA$^-$ *Cells Are Defective in Myosin II Localization in the Front of the Wave*

The cortical localization of myosin II has been implicated in the suppression of lateral pseudopods (Wessels *et al.*, 1988;

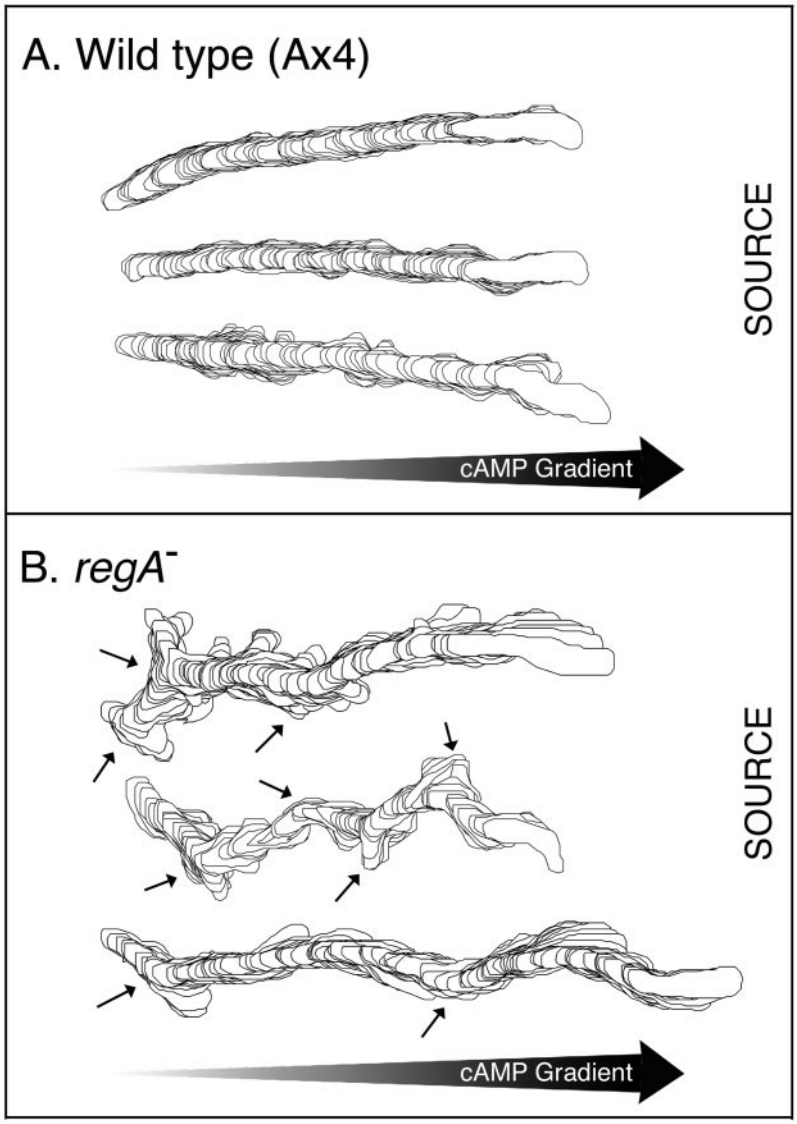

Figure 7. Computer-generated tracks of the three analyzed Ax4 cells and the three analyzed *regA*$^-$ cells in a spatial gradient of cAMP exhibiting the highest chemotactic indices. Small arrows in (B) point to turns initiated by lateral pseudopods.

Spudich, 1989; Wessels and Soll, 1990; Stites *et al.*, 1998; Chung and Firtel, 1999). We, therefore, tested whether myosin II localization to the cell cortex was defective in *regA*$^-$ cells responding to the front of a simulated temporal wave. Ax4 or *regA*$^-$ cells were fixed on the glass wall of a perfusion chamber midway through the third in a series of simulated temporal waves and were stained for myosin II. In Figure 10, confocal images are presented of four representative Ax4 cells (Figure 10, A–D) and four representative *regA*$^-$ cells (Figure 10, E–H). Each image represents an optical section 0.4 μm above the substratum. The great majority of Ax4 cells were elongate, while all of the *regA*$^-$ cells exhibited a flatter, more complex contour, reflecting continued lateral pseudopod formation. In every Ax4 cell (20 were analyzed), myosin was highly localized to the cortex of the posterior three-fourths of the elongate cell body. Localization was extremely weak in the cortex of anterior pseudopods and was weak throughout the interior cytoplasm. *regA*$^-$ cells were analyzed at the same scanning parameters as Ax4 cells. In every *regA*$^-$ cell (20 were analyzed), myosin II was distributed throughout the cytoplasm, rather than localized specifically to the cortex. In a minority of *regA*$^-$ cells, some cortical localization was evident (e.g., Figure 10H), but in all of these cases, staining was still distributed throughout the interior of the cell, except for the nucleus. In Figure 11, the differences in the distribution of myosin II in the front of a simulated temporal cAMP wave are demonstrated by mapping the gray-scale intensity distributions over the scanned areas of a representative Ax4 cell (Figure 11A) and a representative *regA*$^-$ cell (Figure 11B).

DISCUSSION

In the original characterization, it was demonstrated that *regA*$^-$ cultures formed small aggregates and did not form streams, suggesting that cell motility or some other aspect of

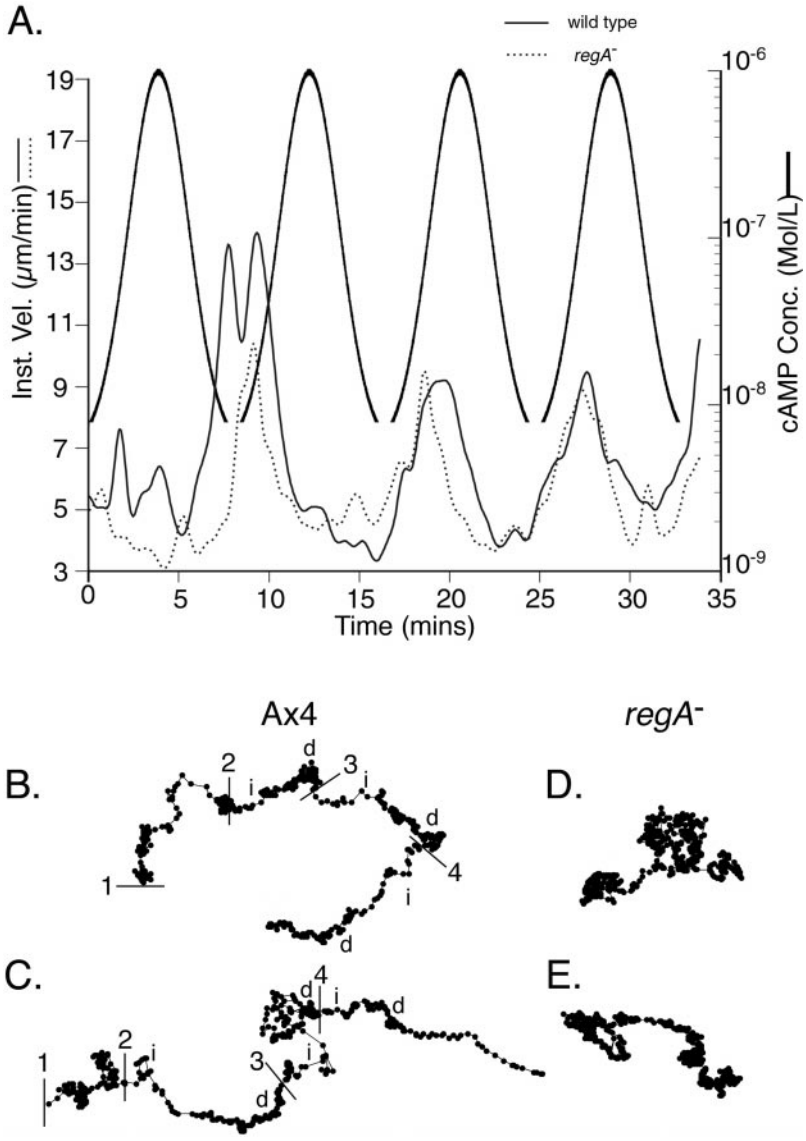

Figure 8. The behavior of Ax4 and *regA*$^-$ cells in temporal gradients of cAMP generated in the absence of spatial gradients that mimic the temporal dynamics of natural waves of cAMP. (A) The average instantaneous velocity and estimated cAMP concentration are shown during simulated waves. Note that neither Ax4 nor *regA*$^-$ cells increase instantaneous velocity in the front of the first simulated wave (Varnum *et al.*, 1985). Instantaneous velocity, measured at 1-min intervals, represents the average of 10 Ax4 cells and 10 *regA*$^-$ cells, respectively. (B and C) The centroid tracks of Ax4 cells responding to sequential simulated temporal waves of cAMP. (D and E) The centroid tracks of *regA*$^-$ cells responding to sequential simulated temporal waves of cAMP. 1, 2, 3, and 4 (in B and C), sequential wave number; i, increasing gradient; d, decreasing gradient. Velocity plots in (A) were smoothed 10 times with Tukey windows of 10, 20, 40, 20, and 10.

the aggregation process was defective (Shaulsky *et al.*, 1996, 1998). We found that mutant cells showed the same developmentally regulated increase in cell motility at the time of aggregation as wild-type cells, and they locomoted in buffer in the absence of a chemotactic signal with motility parameters similar to those of Ax4 cells. These results indicated, therefore, that RegA played no role in the basic motile behavior of cells in the absence of a chemotactic signal.

RegA Is Necessary for Normal Wave Propagation

To identify the defect in *regA*$^-$ aggregation, we first considered whether the production and propagation of chemotactic waves of cAMP might be impaired. RegA is the cAMP phosphodiesterase that reduces the internal concentration of cAMP after the activation of adenylyl cyclase by the G protein-coupled receptor CAR1 (Shaulsky *et al.*, 1996, 1998; Thomason *et al.*, 1998). As such, the loss of RegA might be expected to result in higher intracellular cAMP levels and in persistently high PKA activity. Analysis of the network controlling adenylyl cyclase activity predicts that the loss of RegA would preclude the entrainment of cells such that they would no longer propagate cAMP signals coordinately (Laub and Loomis, 1998). The behavior of Ax4 cells in a predominantly *regA*$^-$ aggregation territory clearly showed that signaling was aberrant. Although *regA*$^-$ cells appeared to release cAMP signals, they were not propagated from a single source even within a small, restricted territory.

RegA Is Not Necessary for Assessing the Direction of a Spatial Gradient of cAMP

We next tested whether *regA*$^-$ cells were capable of chemotaxing in a spatial gradient of cAMP. Mutant and wild-type

Table 3. Number of lateral pseudopods formed by Ax4 and *regA*$^-$ cells in the increasing phases of simulated temporal waves of cAMP

Cell Number	Wave 2	Wave 3	Wave 4	Wave 2 + 3 + 4
Ax4				
1	2	0	1	3
2	2	1	1	4
3	1	1	0	2
4	0	0	0	0
5	0	1	0	1
Mean ± SD		0.7 ± 0.7[a]		2.0 ± 1.6[b]
regA$^-$				
1	5	5	1	11
2	2	4	3	9
3	4	4	4	12
4	3	4	4	11
5	4	3	1	8
6	3	4	6	13
Mean ± SD		3.6 ± 1.2[a]		10.7 ± 1.9[b]

A lateral pseudopod is defined methodologically in the text.

[a] Per wave.

[b] Per three waves.

cells were motion analyzed in a gradient chamber where a steep cAMP gradient is generated by 8 min and then flattens due to diffusion (Shutt *et al.*, 1998; Shutt and Soll, 1999). Peak chemotactic stimulation occurs between ~4 and 14 min (D.S. Shutt and D.R. Soll, unpublished observations). *regA*$^-$ cells exhibited a relatively strong chemotactic response in these spatial gradients of cAMP. Over 90% of *regA*$^-$ cells chemotaxed up the spatial gradient, roughly the same proportion as Ax4 cells. The chemotactic index (±SD) of *regA*$^-$ cells was +0.48 ± 0.28, which is comparable to the chemotactic indices of several other normal strains of *Dictyostelium* (Shutt *et al.*, 1995; Cox *et al.*, 1996) but is lower than that of the parent Ax4 strain. The difference between the chemotactic index of Ax4 and *regA*$^-$ cells was because of a depression in high-end chemotactic indices (i.e., those ≥+0.80). A comparison of the perimeter tracks of Ax4 and *regA*$^-$ cells with the highest chemotactic indices revealed that chemotaxing *regA*$^-$ cells were not as efficient as Ax4 cells in suppressing lateral pseudopod formation (Varnum-Finney *et al.*, 1987b). However, the results clearly demonstrated that RegA is not essential for reading the direction of a spatial gradient and for responding with directed, persistent movement up the gradient.

RegA Is Not Necessary for Recognizing Temporal Changes in cAMP Concentration and Adjusting Instantaneous Velocity Accordingly

Except for the initial decision on direction at the onset of the front of a natural wave, which must be extracted from the spatial dynamics of the wave, all subsequent behavior appears to be dictated by the temporal dynamics of the wave (Figure 1) (Wessels *et al.*, 1992). We, therefore, next tested whether *regA*$^-$ cells responded normally to the temporal dynamics of a natural wave by simulating temporal waves in a round chamber in which spatial gradients of cAMP are not established (Varnum *et al.*, 1985; Varnum-Finney *et al.*, 1987a). We found that mutant cells could distinguish between an increasing versus decreasing temporal gradient of cAMP and adjusted their velocity accordingly, most notably through a positive chemokinetic response in the front of the wave. However, a comparison of the centroid tracks of cells in these perfusion experiments showed that *regA*$^-$ cells made many more turns than wild-type cells and moved chaotically during the increasing phases of the waves. Therefore, although the chemokinetic response was intact, chemotaxis was aberrant.

RegA Is Necessary for Suppressing Lateral Pseudopod Formation in Increasing Temporal Gradients of cAMP

The reason that *regA*$^-$ cells failed to show persistent movement in the increasing phase of a temporal wave of cAMP became obvious when cells were viewed at higher magnification. While Ax4 cells exposed to an increasing temporal gradient of cAMP suppressed lateral pseudopod formation, *regA*$^-$ mutant cells did not. The frequency of lateral pseudopod formation was fivefold higher in mutant cells than in wild-type cells. Such a defect would have severe consequences during natural aggregation. Normal cells select a direction at the beginning of a wave then move for ≥1 min in a relatively blind manner toward the aggregation center in the front of the wave, primarily because lateral pseudopod formation is suppressed by the increasing temporal gradient of cAMP (Figure 1) (Wessels *et al.*, 1992). During the peak and the decreasing phase of a wave, they make no net progress in any direction (Wessels *et al.*, 1992). Therefore, the net progress of cells toward the aggregation center is accomplished in the limited period in the first two-thirds of a wave of cAMP (Wessels *et al.*, 1992). The suppression of lateral pseudopod formation that occurs immediately after the directional decision appears to be essential for directional translocation toward the aggregation center. Loss of that capacity in *regA*$^-$ cells makes them veer off course and disrupts aggregation.

Mechanism of Lateral Pseudopod Suppression

Several cytoskeletal elements have been demonstrated to affect the frequency of lateral pseudopod formation (Wessels *et al.*, 1988; Wessels and Soll, 1990; Wessels *et al.*, 1991; Titus *et al.*, 1992; Wessels *et al.*, 1996). The most dramatic of these is myosin II. Deletion of the myosin II heavy chain gene, *mhcA*, (DeLozanne and Spudich, 1987; Manstein *et al.*, 1989) or the inhibition of the expression of *mhcA* by an antisense construct (Knecht and Loomis, 1987) resulted in the loss of polarity and the extension of pseudopods at equal frequency around the cell perimeter (Wessels *et al.*, 1988; Wessels and Soll, 1990). Because lateral pseudopod formation was normally suppressed in the posterior half of a crawling cell (Varnum-Finney *et al.*, 1987a, b) and myosin II had been demonstrated to be localized there (Yumura and Fukui, 1985), the behavioral phenotype of *mhcA* null mutants was interpreted to indicate that myosin II localized in the cell cortex played a direct role in the suppression of lateral pseudopod formation (Wessels *et al.*, 1988; Spudich, 1989; Wessels and Soll, 1998). Several additional observations supported this interpretation. First, it was demonstrated that *mhcA* null mutant cells exhibited a decrease in cortical ten-

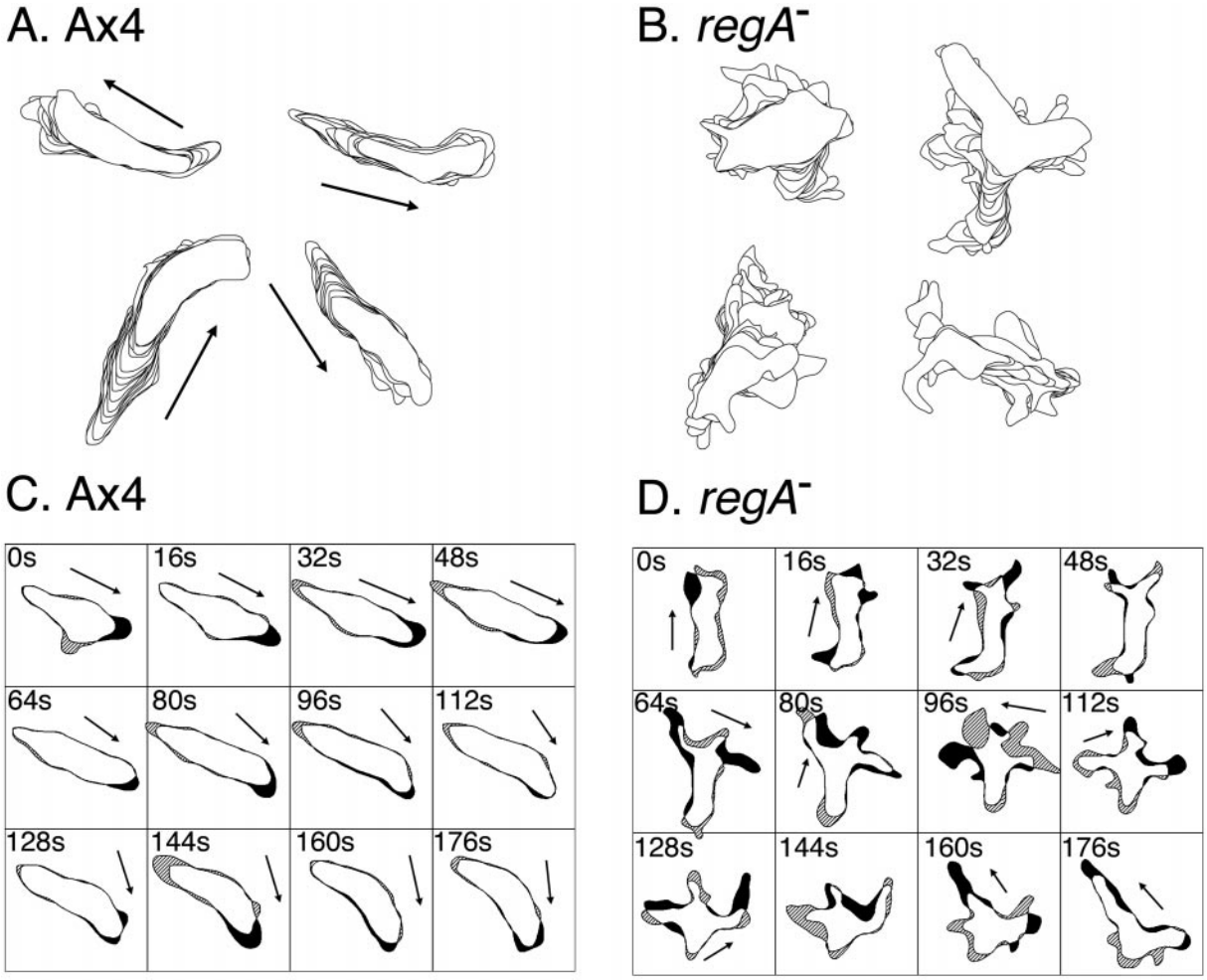

Figure 9. Behavior of Ax4 and *regA*$^-$ cells in the first 3 min of the increasing phase of a temporal wave of cAMP that mimics the temporal dynamics of a natural wave of cAMP. (A and B) Perimeter tracks of Ax4 and *regA*$^-$ cells, respectively. (C and D) Difference pictures of a representative Ax4 and *regA*$^-$ cell, respectively. Black filled areas represent expansion zones, and hatched areas represent contraction zones of difference pictures. Arrows in difference pictures represent direction vectors drawn through the centroids of the earlier and later perimeter image in each difference picture.

sion (Pasternak *et al.*, 1989). Second, conversion of the three mapped threonine phosphorylation sites in the myosin II heavy chain tail to alanines in mutant 3XALA resulted in myosin overassembly (Luck-Vielmetter *et al.*, 1990; Egelhoff *et al.*, 1993), increased cortical tension (Egelhoff *et al.*, 1996), and the abnormal bifurcation of anterior pseudopods during chemotaxis, presumably as a result of increased cortical tension (Stites *et al.*, 1998). Since phosphorylation leads to the dissociation of myosin II filaments in vitro (Kuczmarski and Spudich, 1980; Cote and McCrea, 1987; Ravid and Spudich, 1989), it was suggested that in a normal crawling cell, carefully orchestrated phosphorylation–dephosphorylation of myosin II leads to the disassembly–reassembly, respectively, of myosin II necessary for relocalization in the process of cellular translocation and turning. The movement of myosin II into the cortex, where it polymerizes into thick filaments that generate cortical tension (Pasternak *et al.*, 1989), must be a delicately regulated, cyclical, and localized event that involves the activation of specific kinases and phosphorylases of both myosin heavy chain and light chain (Tan *et al.*, 1992). Our data suggest that RegA may be an essential component in the regulation of this balance in response to temporal gradients of cAMP.

Since RegA is not necessary for reading the direction of a spatial gradient or recognizing a temporal gradient of cAMP, one can assume that the changes in the concentration of intracellular cAMP effected by the deactivation and reactivation of RegA phosphodiesterase activity in the front and back, respectively, of a natural wave are not involved. However, since RegA is essential for suppressing lateral pseudopod formation in response to an increasing temporal gradient of cAMP, one can assume that the periodic changes in intracellular cAMP that result from oscillations in the network that controls RegA activity are coupled to changes in the cell cortex. The myosin II

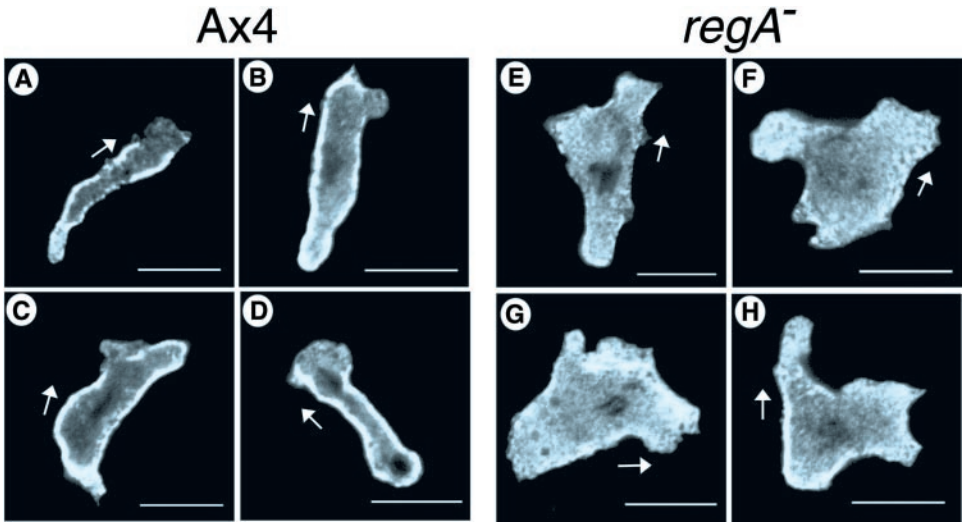

Figure 10. Mysoin II distribution in representative Ax4 cells (A–D) and *regA*$^-$ cells (E–H) midway in the front of a simulated temporal wave of cAMP (the third in a series). Images were taken 0.4 μm off the substratum, using identical confocal scanning parameters for comparison. Small arrows indicate the polarity of the cell interpreted from the parallel DIC image of each cell. The scale bar represents 10 μm.

staining experiments that we have performed demonstrate that *regA* plays a role in regulating the cortical localization of myosin II in the front of a temporal wave of cAMP. The high level of myosin II localization in the cell cortex posterior to the leading edge of an Ax4 amoeba responding to an increasing temporal gradient of cAMP, and the concomitant suppression of lateral pseudopod formation suggest that the high level of cortical tension generated by the localization of myosin II acts as a suppressor of lateral pseudopod formation. The severe reduction in cortical localization in *reg*$^-$ cells in the front of a temporal wave of cAMP demonstrates that RegA plays a direct role in regulating the disassembly–assembly of myosin II leading to cortical localization in response to an increasing temporal waves of cAMP. Since RegA appears to be the major regulator of intracellular cAMP, which in turn regulates the level of PKA activity (Wang and Kuspa, 1997; Loomis, 1998; Aubry and Firtel, 1999), it is reasonable to suggest that RegA functions through PKA to regulate myosin localization through phosphorylation. Although the pathway from PKA to relevant myosin II kinases has not been elucidated, recent evidence suggests that PAKa, a p21-activated Ser/Thr protein kinase, functions as an inhibitor of myosin heavy chain kinase (Chung and Firtel, 1999). The deletion of PAKa has been demonstrated to affect the direction of cellular translocation and to affect the suppression of lateral pseudopod formation in a chemotactic gradient, effects that are quite similar to those resulting from the deletion of RegA. The steps in the pathway beginning with RegA and ending in the phosphorylation/dephosphorylation of myosin II must now be identified.

ACKNOWLEDGMENTS

The authors are indebted to J. Swails for help in assembling the manuscript. The research was supported by National Institutes of Health grants HD-18577 (D.R.S.) and GM52359 (A.K.), and by National Science Foundation grant No. 9728463 (W.F.L.). The authors acknowledge use of the W.M. Keck Dynamic Image Analysis Facility at the University of Iowa funded by the W.M. Keck Foundation.

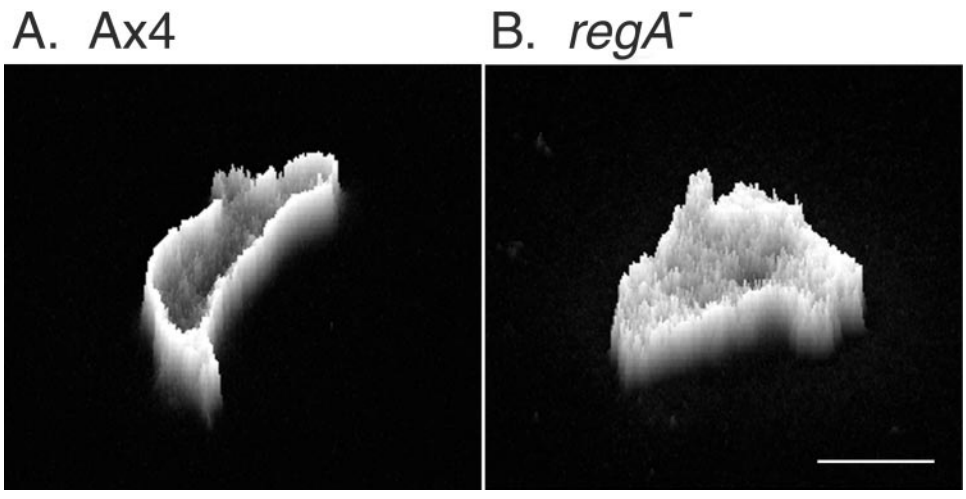

Figure 11. A "pseudo-3D" projection in which the *z*-axis represents the intensity distribution of stained myosin II over the scanned area of a representative Ax4 (Figure 10C) and a representative *regA*$^-$ cell (Figure 10G) midway in the front of a simulated temporal wave of cAMP. Scale bar represents 10 μm.

REFERENCES

Alcantara, F., and Monk, M. (1974). Signal propagation during aggregation in the slime mold *Dictyostelium discoideum*. J. Gen. Microbiol. *85*, 321–334.

Aubry, L., and Firtel, R.A. (1999). Integration of signaling networks that regulate *Dictyostelium* differentiation. Annu. Rev. Cell. Dev. Biol *15*, 469–517.

Chang, W.T., Thomason, P.A., Gross, J.D., and Newell, P.C. (1998). Evidence that the RdeA protein is a component of a multistep phosphorelay modulating rate of development in *Dictyostelium*. EMBO J. *17*, 2809–2816.

Chung, C.Y., and Firtel, R.A. (1999). PAKa, a putative PAK family member, is required for cytokinesis and the regulation of the cytoskeleton in *Dictyostelium discoideum* cells during chemotaxis. J. Cell Biol. *147*, 559–575.

Cocucci, S., and Sussman, M. (1970). RNA in cytoplasmic and nuclear fractions of cellular slime mold amoebae. J. Cell Biol. *45*, 399–407.

Cote, G.P., and McCrea, S.M. (1987). Selective removal of the carboxyl-terminal end of the *Dictyostelium* myosin II heavy chain by chymotrypsin. J. Biol. Chem. *262*, 13033–13038.

Cox, D., Wessels, D., Soll, D.R., Hartwig, J., and Condeelis, J. (1996). Re-expression of ABP-120 rescues cytoskeletal, motility and phagocytosis defects of ABP-120-*Dictyostelium* mutants. Mol. Biol. Cell *7*, 803–823.

Devreotes, P.N. (1982). Chemotaxis. In: The development of Dictyostelium discoideum, ed. W. F. Loomis, New York, NY: Academic Press, 117–168.

Devreotes, P.N., Potel, M.J., and MacKay, S.J. (1983). Quantitative analysis of cAMP waves mediating aggregation in *Dictyostelium discoideum*. Dev. Biol. *96*, 405–415.

DeLozanne, A., and Spudich, J.A. (1987). Disruption of the *Dictyostelium* myosin heavy chain gene by homologous recombination. Science *236*, 1086–1091.

Egelhoff, T.T., Lee, R.J., and Spudich, J.A. (1993). *Dictyostelium* myosin heavy chain phosphorylation sites regulate myosin filament assembly and localization in vivo. Cell *75*, 363–371.

Egelhoff, T.T., Naismith, T.V., and Brozovich, F.V. (1996). Myosin-based cortical tension in *Dictyostelium* resolved into heavy and light chain-regulated components. J. Muscle Res. Cell Motil. *17*, 269–274.

Escalante, R., Wessels, D., Soll, D.R., and Loomis, W.F. (1997). Chemotaxis to cAMP and slug migration in *Dictyostelium* both depend on MigA, a BTB protein. Mol. Biol. Cell *8*, 1763–1775.

Fisher, P.R., Merkl, R., and Gerisch, G. (1989). Quantitative analysis of cell motility and chemotaxis in *Dictyostelium discoideum* by using an image processing system and a novel chemotaxis chamber providing stationary chemical gradients. J. Cell Biol. *108*, 973–984.

Franke, J., and Kessin, R.H. (1992). The cyclic nucleotide phosphodiesterases of *Dictyostelium discoideum*: molecular genetics and biochemistry. Cell. Signal. *4*, 471–478.

Gerisch, G., Hulser, D., Malchow, D., and Wick, U. (1975). Cell communication by periodic cyclic AMP pulses. Philos. Trans. R. Soc. Lond. B Biol. Sci. *272*, 181–192.

Harwood, A.J., and Drury, L. (1990). New vectors for expression of the *E. coli lacZ* gene in *Dictyostelium*. Nucleic Acids Res. *18*, 4292.

Hong, K., Nishiyama, M., Henley, J., Tessier-Lavigne, M., and Poo, M. (2000). Calcium signaling in the guidance of nerve growth by netrin-1. Nature *403*, 93–99.

Jin, T., Zhang, N., Long, Y., Parent, C., and Devreotes, P.N. (2000). Localization of the G protein complex in living cells during chemotaxis. Science *287*, 1034–1036.

Knecht, D., and Loomis, W.F. (1987). Antisense RNA inactivation of myosin heavy chain gene expression in *Dictyostelium discoideum*. Science *236*, 1081–1085.

Konijn, T.M., Van de Meene, Bonner, J.T., and Barkley, D.S. (1967). The acrasin activity of adenosine-3′, 5′-cyclic phosphate. Proc. Natl. Acad. Sci. USA *58*, 1152–1154.

Kuczmarski, E.R., and Spudich, J.A. (1980). Regulation of myosin self-assembly: phosphorylation of heavy chain inhibits formation of thick filaments. Proc. Natl. Acad. Sci. USA, *77*, 7292–7296.

Laub, M., and Loomis, W.F. (1998). A molecular network that produces spontaneous oscillations in excitable cells of *Dictyostelium*. Mol. Biol. Cell *9*, 3521–3532.

Loomis, W.F. (1998). Role of PKA in timing of developmental events in *Dictyostelium* cells. Microbiol. Mol. Biol. Rev. *62*, 684–694.

Luck-Vielmetter, D., Schleicher, M., Grabatin, B., Wippler, J., and Gerisch, G. (1990). Replacement of threonine residues by serine and alanine in a phosphorylatable heavy chain fragment of *Dictyostelium* myosin II. FEBS Lett. *269*, 239–243.

Maeda, M., Aubry, L., Insall, R., Gaskins, C., Devreotes, P.N., and Firtel, R.A. (1996). Seven helix chemoattractant receptors transiently stimulate mitogen-activated protein kinase in *Dictyostelium*: role of heterotrimeric G proteins. J. Biol. Chem. *271*, 3351–3354.

Manstein, D.J., Titus, M.A., De Lozanne, A., and Spudich, J. (1989). Gene replacement in *Dictyostelium*: generation of myosin null mutants. EMBO J. *8*, 923–932.

Nellen, W., and Firtel, R.A. (1985). High-copy-number transformants and co-transformation in *Dictyostelium*. Gene *39*, 155–163.

Parent, C., and Devreotes. P.N. (1996). Molecular genetics of signal transduction. Annu. Rev. Biochem. *65*, 411–440.

Pasternak, C. Spudich, J.A., Elson, E.J. (1989). Capping of surface receptors and concomitant cortical tension are generated by conventional myosin. Nature *341*, 541–549.

Ravid, S., and Spudich, J.A. (1989). Myosin heavy chain kinase from developed *Dictyostelium* cells: purification and characterization. J. Biol. Chem. *264*, 15144–15150.

Segall, J., Ecke, M., Kuspa, A., Shaulsky, G., Maeda, M., Gaskin, C., Firtel, R.A., and Loomis, W.F. (1995). A MAP kinase necessary for receptor mediated activation of adenylyl cyclase in *Dictyostelium*. J. Cell Biol. *128*, 405–413.

Servant, G., Weiner, O.D., Herzmark, P., Balla, T., Sedat, J.W., and Bourne, H.R. (2000). Polarization of chemoattractant receptor signaling during neutrophil chemotaxis. Science *287*, 1037–1040.

Shaffer, B.M. (1962). The acrasina. Adv. Morphog. *2*, 109–182.

Shaulsky, G., Escalante, R., and Loomis, W.F. (1996). Developmental signal transduction pathways uncovered by genetic suppressors. Proc. Natl. Acad. Sci. USA *93*, 15260–152665.

Shaulsky, G., Fuller, D., and Loomis, W.F. (1998). A cAMP-phosphodiesterase controls PKA-dependent differentiation. Development *125*, 691–699.

Shutt, D.C., Jenkins, L.M., Daniels, K., Kennedy, R., Stapleton, J., and Soll, D.R. (1998). T cell syncytia induced by HIV release T cell chemoattractants: demonstration with a newly developed single cell chemotaxis. J. Cell Sci. *111*, 99–109.

Shutt, D., and Soll, D.R. (1999). Nef and tat function together as a two component T cell chemoattractant released by HIV-induced syncytia. J. Cell Sci. *112*, 3931–3941.

Shutt, D., Wessels, D., Chandrasekhar, A., Luna, B., Hitt, A., and Soll, D.R. (1995). Ponticulin plays a role in the spatial stabilization of pseudopods. J. Cell Biol. *131*, 1495–1506.

Soll, D.R. (1979). Timers in developing systems. Science *203*, 841–849.

Soll, D.R. (1987). Methods for manipulating and investigating developmental timing in *Dictyostelium discoideum*. In: Methods in Cell Biology, ed. J. Spudich, New York, NY: Academic Press, 413–431.

Soll, D.R. (1989). Behavioral studies into the mechanism of eukaryotic chemotaxis. J. Chem. Ecol. *16*, 133–150.

Soll, D.R. (1995). The use of computers in understanding how cells crawl. Int. Rev. Cytol. *163*, 43–104.

Soll, D.R. (1999). 3D reconstruction and motion analysis of the surface and internal architecture of live, crawling cells: 3D-DIAS. Comput. Med. Imaging Graph. *23*, 3–14.

Soll, D.R., and Voss, E. (1998). Two and three dimensional computer systems for analyzing how cells crawl. In: Motion Analysis of Living Cells, ed. D.R. Soll, D. Wessels, New York, NY: John Wiley, 25–52.

Soll, D.R., Wessels, D., and Sylwester, A. (1993). The motile behavior of amoebae in the aggregation wave in *Dictyostelium discoideum*. In: Experimental and Theoretical Advances in biological Pattern Formation, eds. H.G. Othmer, P. K. Maini, and J.D. Murray, New York, NY: Plenum Press, 325–338.

Spudich, J.A. (1989). In pursuit of myosin function. Cell. Regul. *1*, 1–11.

Stites, J., Wessels, D., Uhl, A., Egelhoff, T., Shutt, D., and Soll, D.R. (1998). Phosphorylation of the *Dictyostelium* myosin II heavy chain is necessary for maintaining cellular polarity and suppressing turning during chemotaxis. Cell Motil. Cytoskeleton *39*, 31–51.

Sussman, M. (1987). Cultivation and synchronous morphogenesis of *Dictyostelium* under controlled experimental conditions. Methods Cell Biol. *28*, 9–30.

Tan, J.L., Ravid, S., and Spudich, J.A. (1992). Control of nonmuscle myosins by phosphorylation. Annu. Rev. Biochem. *61*, 721–759.

Tamagnone, L., Artigiani, S., Chen, H., He, Z., Ming, G.I, Song, H., Chedotal, A., Winberg, M.L., Goodman, C.S., Poo, M., Tessier-Lavigne, M., and Comoglio, P.M. (1999). Plexins are a large family of receptors for transmembrane, secreted, and GPI-anchored semaphorins in vertebrates. Cell *99*, 71–80.

Titus, M., Wessels, D., Spudich, J., and Soll, D.R. (1992). The unconventional myosin encoded by the *myo A* gene plays a role in *Dictyostelium* motility. Mol. Biol. Cell *4*, 233–246.

Thomason, P., Traynor, D., Cavet, G., Chang, W.T., Harwood, A., and Kay, R. (1998). An intersection of the cAMP/PKA and two component signal transduction system in *Dictyostelium*. EMBO J. *17*, 2838–2845.

Tomchik, S.J., and Devreotes, P.N. (1981). cAMP waves in *Dictyostelium discoideum*: demonstration by an isotope dilution fluorography technique. Science *212*, 443–446.

Van Haastert, P.J.M. (1983). Sensory adaptation of *Dictyostelium discoideum* cells to chemotactic signals. J. Cell Biol. *96*, 1559–1565.

Van Haastert, P.J.M., and Kuwayama, H. (1997). cGMP as second messenger during *Dictyostelium* chemotaxis. FEBS Lett. *410*, 25–28.

Varnum, B., Edwards, K., and Soll, D.R. (1985). *Dictyostelium* amoebae alter motility differently in response to increasing versus decreasing temporal gradients of cAMP. J. Cell Biol. *101*, 1–5.

Varnum, B., and Soll, D.R. (1984). Effect of cAMP on single cell motility in *Dictyostelium*. J. Cell Biol. *99*, 1151–1155.

Varnum-Finney, B., Edwards, K., Voss, E., and Soll, D.R. (1987a). Amoebae of *Dictyostelium discoideum* respond to an increasing temporal gradient of the chemoattractant cAMP with a reduced frequency of turning: evidence for a temporal mechanism in amoeboid chemotaxis. Cell Motil. Cytoskeleton *8*, 7–17.

Varnum-Finney, B., Voss, E., and Soll, D.R. (1987b). Frequency and orientation of pseudopod formation of *Dictyostelium discoideum* amoebae chemotaxing in a spatial gradient: further evidence for a temporal mechanism. Cell Motil. Cytoskeleton *8*, 18–26.

Wang, B., and Kuspa, A. (1997). *Dictyostelium* development in the absence of cAMP. Science *277*, 251–254.

Wang, Y., Liu, J., and Segall, J.E. (1998). MAP kinase function in amoeboid cells. J. Cell Sci. *111*, 373–383.

Wessels, D., Murray, J., Jung, G., Hammer, J., and Soll, D.R. (1991). Myosin IB null mutant of *Dictyostelium* exhibits abnormalities in motility. Cell Motil. Cytoskeleton *20*, 301–315.

Wessels, D., Murray, J., and Soll, D.R. (1992). The complex behavior cycle of chemotaxing *Dictyostelium* amoebae is regulated primarily by the temporal dynamics of the natural wave. Cell Motil. Cytoskeleton *23*, 145–156.

Wessels, D., Schroeder, N., Voss, E., Hall, A., Condeelis, J., and Soll, D.R. (1989). cAMP mediated inhibition of intracellular particle movement and actin reorganization in *Dictyostelium*. J. Cell Biol. *109*, 2841–2851.

Wessels, D., and Soll, D.R. (1990). Myosin II heavy chain null mutant of *Dictyostelium* exhibits defective intracellular particle movement. J. Cell Biol. *111*, 1137–1148.

Wessels, D., and Soll, D.R. (1998). Computer-assisted analysis of cytoskeletal mutants of *Dictyostelium*. In: Motion Analysis of Living Cells, ed. D.R. Soll and D. Wessels, New York, NY: John Wiley, 101–140.

Wessels, D., Soll, D.R., Knecht, D., Loomis, W.F., DeLozanne, A., and Soll, D.R. (1988). Cell motility and chemotaxis in *Dictyostelium* amebae lacking myosin heavy chain. Dev. Biol. *128*, 164–177.

Wessels, D., Titus, M., and Soll, D.R. (1996). A *Dictyostelium* myosin I. plays a crucial role in regulating the frequency of pseudopods formed on the substratum. Cell Motil. Cytoskeleton *33*, 64–79.

Wessels, D., Voss, E., von Bergen, N., Burns, R., Stites, J., and Soll, D.R. (1998). A computer-assisted system for reconstructing and interpreting the dynamic three-dimensional relationships of the outer surface, nucleus, and pseudopods of crawling cells. Cell Motil. Cytoskeleton *41*, 225–246.

Yumura, S., and Fukui, Y. (1985). Reversible cyclic AMP-dependent change in distribution of myosin thick filaments in *Dictyostelium*. Nature *314*, 194–196.

Zigmond, S.H. (1977). The ability of polymorphonuclear leukocytes to orient in gradients of chemotactic factors. J. Cell Biol. *75*, 606–616.